HHS Public Access

A Fbxo48 inhibitor prevents pAMPKα degradation and ameliorates insulin resistance

Yuan Liu[1,2,3,†,*], **Michael J. Jurczak**[4], **Travis B. Lear**[1,2,7], **Bo Lin**[1], **Mads B. Larsen**[1], **Jason R. Kennerdell**[1], **Yanwen Chen**[1], **Brydie R. Huckestein**[4], **Matthew K. Nguyen**[1], **Ferhan Tuncer**[1], **Yu Jiang**[5], **Satdarshan P. Monga**[6], **Christopher P. O'Donnell**[2], **Toren Finkel**[1,7], **Bill B. Chen**[1,2,7,†,*], **Rama K. Mallampalli**[8,†,*]

[1]Aging Institute, University of Pittsburgh/UPMC, Pittsburgh, PA 15219, USA

[2]Department of Medicine, Division of Pulmonary, Allergy and Critical Care Medicine, University of Pittsburgh, Pittsburgh, PA 15213 USA

[3]The McGowan Institute for Regenerative Medicine, Pittsburgh, PA 15219 USA

[4]Division of Endocrinology and Metabolism, University of Pittsburgh, Pittsburgh, PA 15213 USA

[5]Department of Pharmacology and Chemical Biology, University of Pittsburgh, Pittsburgh, PA 15261 USA

[6]Department of Pathology and Medicine, and Pittsburgh Liver Research Center, University of Pittsburgh and University of Pittsburgh Medical Center, Pittsburgh, PA 15213 USA

[7]Vascular Medicine Institute, University of Pittsburgh, Pittsburgh, PA 15213 USA

[8]Department of Internal Medicine, The Ohio State University Wexner Medical Center, Columbus, OH 43210 USA

Abstract

The AMP-activated protein kinase (Ampk) is a central regulator of metabolic pathways and increasing Ampk activity has been considered to be an attractive therapeutic target. Here, we identified an orphan ubiquitin E3 ligase subunit protein, Fbxo48, that targets the active, phosphorylated Ampkα (pAmpkα) for polyubiquitylation and proteasomal degradation. We generated a novel Fbxo48 inhibitory compound, BC1618, whose potency in stimulating Ampk-dependent signaling greatly exceeds AICAR or metformin. This compound increases the biological activity of Ampk not by stimulating the activation of Ampk, but rather by preventing

*Correspondence to: liuy13@upmc.edu, chenb@upmc.edu, rama.mallampalli2@osumc.edu.
†These authors contributed equally to this work.

activated pAmpkα from Fbxo48-mediated degradation. We demonstrate that consistent with augmenting Ampk activity, BC1618 promotes mitochondrial fission, facilitates autophagy, and improves hepatic insulin sensitivity in high fat diet-induced obese mice. Hence, we provide a unique bioactive compound that inhibits pAmpkα disposal. Together, these results define a new pathway regulating Ampk biological activity and demonstrate the potential utility of modulating this pathway for therapeutic benefit.

Keywords

Ampk; energetics; diabetes

Introduction

5'-AMP-activated protein kinase (Ampk), is positioned at the nexus of metabolic signaling pathways, sensing fluctuations in cellular energy supply to acutely modulate the balance of catabolic and anabolic processes [1]. Evidence suggests that following a wide range of perturbations including starvation, hypoxia, impaired mitochondrial function, and disease states such as type 2 diabetes (T2D), Ampk is responsible for orchestrating the global response to energetic stress in order to enact beneficial physiological changes [2]. As such, pharmacologic Ampk activation provides a highly attractive and widely studied therapeutic option for multiple disorders [3]. Ampk is a heterotrimeric protein kinase comprised of an alpha (α) catalytic subunit in a molecular complex with a beta (β) scaffolding subunit and a gamma (γ) regulatory subunit [4]. These subunits are encoded by seven distinct genes enabling the formation of a twelve unique αβγ heterotrimeric combinations. The composition of Ampk heterotrimeric complexes differs between species, as well as differing across various tissues within a given species. Activation of Ampk involves phosphorylation of a conserved threonine residue (referred to as Thr172) located within the catalytic core of the Ampk α subunit. In mammals, this phosphorylation event is often catalyzed by either calcium/calmodulin dependent protein kinase (CaMKK) β or liver kinase B1 (LKB1). Phosphorylation of the α subunit results in an increase in Ampk activity by 2–3 order of magnitude [5]. Ampk can be further activated allosterically by the direct binding of AMP to the γ subunit. As such, to date, small molecules that activate Ampk can be broadly divided into three distinct categories: (1) compounds that increase intracellular AMP and ADP thereby indirectly activating Ampk; (2) agents mimicking AMP that bind to the Ampk γ subunit; (3) or compounds selectively binding the interface between Ampk α and β subunits [5]. The first class of molecules is exemplified by the widely used agent metformin, which appears to exert its beneficial effects largely through an alteration in mitochondrial activity leading to increases in AMP levels and subsequent Ampk activation [6]. Compounds such as AICAR, which are analogues of AMP, are typical of the second class of Ampk activators. Finally, the third class of molecules have been the subject of intense investigation since the discovery in 2006 of the first non-nucleotide, direct small molecule AMPK activator [7]. This agent, and subsequent follow on molecules, bind directly to the heterotrimeric complex and induce a conformational change leading to increased Ampk activity through multiple mechanisms including allosteric modulation, increased Thr172 phosphorylation, or reduced Thr172 dephosphorylation. In general, this newer class of small molecule activators

has the capacity to activate each of the 12 different Ampk heterotrimeric complexes, although the degree of activation can vary based on the particular β subunit expressed within the complex. Nonetheless, these pan-Ampk activators are not without their own set of liabilities. In particular, certain members of this class appear to induce cardiac hypertrophy after administration to rodent and non-human primate species [8]. This observation likely relates to the fact that in humans, a number of dominantly-inherited gain-of-function mutations have been identified in the γ2 subunit (PRKAG2) that lead to a constellation of cardiac abnormalities including left ventricular hypertrophy, glycogen accumulation and arrhythmias [9]. Thus, while activation of Ampk is desirable, constitutive activation can also result in a number of untoward side-effects.

As delineated above, the vast majority of strategies to increase Ampk activity have revolved on using small molecules as a means to increase activation of Ampk. However, it remains possible that after Ampk is activated, one could potentially use small molecules to prevent the deactivation of the kinase. Such efforts could potentially revolve around preventing Ampk dephosphorylation by inhibiting intracellular phosphatases, and attempts exploiting this approach have been recently described [10]. Here, we report a new biological mechanism regulating Ampk deactivation. In particular, we demonstrate that activation by Thr172 phosphorylation generates a phospho-degron signal leading to ubiquitin-dependent degradation of the activated form of Ampk. We herein identify the relevant E3 ubiquitin ligase and show that a small molecule that inhibits interaction between this E3 ubiquitin ligase complex and the α subunit of Ampk results in prolonged activation of Ampk both *in vitro* and *in vivo*. One particular compound described, BC1618, appears to be approximately 1000-fold more potent than metformin and is extremely well-tolerated in mice. Thus, we delineate a new strategy to generate a pan-AMPK activator that leverages a heretofore unknown mode of regulation, namely the E3 ligase-dependent degradation of activated Ampk.

Results

SCF^{Fbxo48} mediates pAmpkα ubiquitination and degradation

Metformin has been used for nearly a century and is now the most commonly prescribed oral anti-diabetic drug worldwide. Metformin activates Ampk via increasing cellular AMP/ADP levels by inhibiting mitochondrial respiration and ATP production [11]. Consistent with numerous reports, we also observed that glucose depletion elevated Thr172 pAmpkα protein levels in primary and immortalized human bronchial epithelial cells (BEAS-2B), and overnight incubation of metformin in the culture medium further augmented this effect dose-dependently (Supplementary Fig. 1A). However surprisingly, total Ampkα protein levels correspondingly decreased. We next measured Ampkα protein levels in Lkb1 (Ampk activating kinase in response to energy stress) depleted cells and control cells [12, 13]. *ShRNA-mediated* Lkb1 silencing abrogated glucose starvation-induced Ampkα phosphorylation, while preserving total Ampkα protein levels (Supplementary Fig. 1B). These data suggest that Thr172 phosphorylation may drive the degradation of Ampkα. Indeed, the rapid degradation of pAmpkα that occurred within 30 min was reversed by addition of the proteasome inhibitor carfilzomib (Fig.

1A, Supplementary Fig. 1C). In contrast, the lysosome inhibitor leupeptin did not impact pAmpkα degradation. Plasmid-mediated ectopic expression of a phospho-null T172A Ampkα2 mutant was resistant to cycloheximide (CHX)-induced protein degradation (Supplementary Fig. 1D), suggesting that phosphorylation of Thr172 might prime Ampkα for 26S proteasome-dependent degradation. To explore whether pAmpkα degradation was ubiquitin-dependent, we performed anti-ubiquitin TUBE-based pulldown assays and observed that glucose starvation increases polyubiquitylated pAmpkα and the proteasome inhibitor MG132 further enhanced polyubiquitylated pAmpkα levels (Fig. 1B). Similarly, metformin treatment dose-dependently increased polyubiquitylated pAmpkα (Extended Data Fig. 1A). We further noticed that *in vivo* glucose starvation also increased polyubiquitylated pAmpkα in mouse liver (Extended Data Fig. 1B). Finally, compared to the WT protein, the stable phospho-null T172A mutant had lower levels of ubiquitination (Extended Data Fig. 1C). The introduction of a ubiquitin docking deficient Ampkα K60R mutation stabilized Ampkα, further confirming that Ampkα degradation was ubiquitin dependent (Supplementary Fig. 1E).

To identify the ubiquitin E3 ligase class that is involved in pAmpkα ubiquitylation, we employed a Cullin-RING ligase (CRL) inhibitor, MLN4924 (currently in phase II clinical trials for cancer) [14]. MLN4924 increased pAmpkα protein abundance (Extended Data Fig. 2A) and extended pAmpkα protein half-life (Extended Data Fig. 2B), suggesting that CRLs may participate in regulating pAmpkα protein stability. Through unbiased RNA-sequencing, we identified several candidate F-box proteins, the key substrate recognition modules within Skp1-Cul1-based CRL1 E3 ligases, which exhibited lower expression, corresponding to elevated pAmpkα protein levels during glucose depletion (Extended Data Fig. 2C). Further examination of the down-regulated F-box proteins led to the observation that overexpression of a previously uncharacterized *Fbxo48* selectively decreased pAmpkα protein levels (Extended Data Fig. 3A–C). In vitro ubiquitinylation reactions using recombinant proteins indicated that Ampkα was polyubiquitinylated by Fbxo48 (Extended Data Fig. 3D). Detailed protein dynamic analysis demonstrated that in response to glucose starvation, the protein abundance of Fbxo48 declined, whereas pAmpkα protein levels concomitantly increased (Fig. 1C, Supplementary Fig. 2A). Transient *Fbxo48* expression in cells also dose-dependently decreased both phospho and total Ampkα protein levels (Fig. 1D). To test if Fbxo48 was an authentic E3 ligase subunit [15], we performed immunoprecipitation and detected V5-tagged Fbxo48 in a complex with the CRL1 E3 catalytic core Skp1-Cul1 (Fig. 1E). The direct interaction between Fbxo48 and Ampkα was further confirmed in peptide binding assays (Fig. 1F). Both phosphorylated and phospho-mimetic (T→D) Ampkα peptides bound to Fbxo48, and a phospho-null (T→A) form of Ampkα peptide substantially decreased Fbxo48 binding affinity. *Fbxo48* overexpression also accelerated pAmpkα protein degradation (Fig. 1G), whereas *Fbxo48* knockdown prolonged pAmpkα protein half-life (Fig. 1H). Lastly, *Fbxo48* knockdown significantly augmented Ampk activation during the first 10min of glucose starvation (Fig. 1I, Supplementary Fig. 2B). These studies suggest that Fbxo48 negatively regulates glucose starvation induced pAmpk activation.

To understand whether the pathway described might be relevant for human disease we analyzed liver samples of patients with non-alcoholic fatty liver disease (NAFLD). This metabolic condition is reaching epidemic proportions, and affected individuals display lipid

accumulation in the liver, contributing to the development of T2D, CVD and non-alcoholic steatohepatitis (NASH) [16]. Compared to control non-hepatitis liver (NHL), higher levels of Fbxo48 protein were observed in NASH patient liver tissues, while lower levels of both phospho and total Ampkα protein levels were noted (Supplementary Fig. 3A, B, C). Together, these observations demonstrate that Fbxo48 functions as the substrate-recruiting subunit in SCF type E3 ligases to ubiquitylate pAmpkα for proteasomal degradation, providing a unique mechanism of action and potential therapeutic target to preserve cellular pAmpkα protein concentrations.

Small molecule Fbxo48 inhibitors increase pAmpkα

Through a homology model, we determined that Fbxo48 contains a major cavity with potential for substrate targeting. We hypothesized that a small molecule inhibitor of this Fbxo48 cavity would disrupt Fbxo48/pAmpkα interaction and preserve pAmpkα protein levels. Using molecular docking analysis and score-ranking operations, we assessed potential ligands for the Fbxo48 domain cavities (Supplementary Fig. 4A). Through the LibDock program from Discovery Studio 3.5, we conducted an *in silico* screen of 3 million potential ligands for the Fbxo48 pocket. Initially, 16 compounds were selected and assessed for their ability to increase pAmpkα protein levels (Supplementary Fig. 4B–C). One of the most potent compounds, BC1583 (1), was further selected for additional testing. Figure S4A indicates the *in silico* docking model for BC1583 bound to Fbxo48. To evaluate BC1583 efficacy, we employed the well-recognized AMP-mimic pAmpkα activator, AICAR [17]. As expected, AICAR dose-dependently increased pAmpkα protein levels under glucose starvation (Fig. 2A). Moreover, the addition of BC1583 synergistically increased pAmpkα protein levels to a greater extent than AICAR alone. BC1583 also elevated protein abundance of phosphorylated acetyl-CoA carboxylase (pACC), an Ampk downstream substrate [18]. Of note, BC1583 alone at 4 μM increased pAmpkα and pACC levels, an effect that exceeded AICAR treatment at 250 μM. We excluded the possibility that BC1583 acts by either increasing Ampkα kinase Lkb1 or decreasing Ampkα phosphatase PP2C (Fig. 2B). Although BC1583 exhibited excellent activity in cells, prediction models (Lipinski's rule of five) of physiochemical properties suggested poor bioavailability. Thus, we assessed the structure-activity relationship (SAR) to identify and characterize other similar, but simplified compounds derived from BC1583 (Supplementary Fig. 5A–B). BC1583 is a relatively large molecule with MW of 617Da. It contains benzene-1,4-diol moiety with two symmetric 1-(dibenzylamino)propan-2-ol groups. We hypothesize that asymmetric structure with only one 1-(dibenzylamino)propan-2-ol group is sufficient for activity. Compounds showed in Supplementary Fig. 5A were specifically selected to confirm this hypothesis. From this SAR study, we further determined that symmetric dibenzylamino moiety is also important for activity. Finally, we introduced trifluoromethyl group to improve compound metabolic stability and PK profile which led to the lead molecule, labeled BC1618 (**2**) (Fig. 2C) (mass-spectrometry and NMR shown in Supplementary Fig. 6). BC1618 exhibits significantly better potency compared to all other SAR compounds and original hit molecule BC1583 towards increase pAmpkα protein measured by an in-cell ELISA assay (Supplementary Fig. 5B). BC1618 enhanced pAmpkα protein stability during CHX treatment (Fig. 2D). BC1618 displayed more than a 1000-fold enhanced activity than metformin to stimulate pAmpkα in cells (Fig. 2E). BC1618-induced dose- and time-

dependent increases in pAmpkα and pACC protein levels were also confirmed in human primary-like hepatocytes (HepaRG; Supplementary Fig. 7A, B).

Fbxo48 inhibitor interrupts Fbxo48/pAmpkα interaction

At 1 μM, BC1618 effectively disrupted the interaction between Fbxo48 and pAmpkα (Fig. 3A, B). However, BC1618 had no effects on Fbxo48, Ampkα1 or Ampkα2 mRNAs (Supplementary Fig. 8A), nor did it alter ADP/ATP ratios in cells (Supplementary Fig. 8B). Further, BC1618 directly interacted with Fbxo48 but not Fbxo30 (negative control) when measured by a Cellular Thermal Shift Assay (CETSA) (Fig. 3C) [19–21]. Dose-dependent BC1618-mediated increases in pAmpkα levels were not observed in *siRNA*-mediated Fbxo48 knockdown cells and in the knockdown cells, pAmpkα protein remained basally elevated but unchanged with increasing amounts of BC1618 (Fig. 3D, Supplementary Fig. 8C). These observations are consistent with BC1618 elevating pAmpkα levels by inhibiting Fbxo48. To further assess off-target effects, a kinase screen was performed to demonstrate that BC1618 did not exert significant modulatory effects on other essential kinases (Extended Data Fig. 4).

To further characterize the specificity of BC1618, we performed quantitative phosphoproteomics on BEAS-2B cells treated with BC1618 in triplicate and compared this to vehicle-treated controls. Our mass spectrometry dataset comprises 4772 phosphosites in 1724 proteins (Extended Data Fig. 5A–B). We used this data to examine if BC1618 resulted in similarities to known phosphoprotein signatures using PTM-SEA [22], with the expectation that this would provide an unbiased assessment of BC1618 activity, and would identify other perturbations and pathways similar to BC1618. Interestingly, one of the most significantly upregulated signatures was associated with PERT-PSP_RAPAMYCIN, suggesting BC1618 has at least some activities in common with rapamycin treatment (Extended Data Fig. 5C). Additionally, the KINASE-PSP_AMPKA1/PRKAA1 was also upregulated, this signature includes phosphosites associated with targets of AMPK. The most downregulated signature was KINASE-PSP_mTOR/MTOR, which includes phosphosites that are targets of mTOR, the target of rapamycin Supplementary Fig. 9. An AMPK activator would be expected to downregulate mTOR activity due to direct and indirect inhibition of mTOR by AMPK [23]. Thus, these observations are consistent with BC1618 activating AMPK to affect phosphorylation in a manner similar to rapamycin. The PERT-PSP_ANTI_CD3 signature refers to phosphosites downstream of T cell receptor activation by an antibody that crosslinks CD3 [24]. As T cell receptor activation activates AMPK, it is perhaps not surprising that the two stimuli would have similar effects on the phosphoproteome [25]. The PERT-PSP_PHORBOL_ESTER signature also may be explained in terms of AMPK activation, as treatment with phorbol ester results in AMPK activation [26].

BC1618 facilitates mitochondria fission and autophagy

Consistent with a previous study showing Ampk activation regulates mitochondrial dynamics by phosphorylating Mff [27], we observed that BC1618 increased mitochondrial fission using confocal microscopy combined with Mito Tracker staining (Fig. 4A). Correspondingly, BC1618 increased phospho-Mff (pMff) protein levels (Fig. 4B). Emerging

studies have demonstrated that Ampk has important roles in regulating autophagy by directly phosphorylating autophagy-initiating protein kinase Ulk1 and by suppressing mTORC1 activity through phosphorylating Raptor [28, 29]. BC1618 increased abundance of a series of autophagic marker proteins during glucose depletion (Supplementary Fig. 9A) [30]. Specifically, BC1618 induced phosphorylation of the mTORC1 associated protein Raptor, reducing pS6 levels, all consistent with the known mTOR inhibitory effects exerted by activated Ampk (Fig. 4C, Supplementary Fig. 9A). Glucose depletion-induced autophagy increases phospho-Ulk1 (pUlk1) and the ratio of LC3B II:I [31], and BC1618 further enhanced this effect and dose-dependently increased the autophagy marker pUlk1 (Fig. 4D) and the LC3B II:I ratio (Supplementary Fig. 9B). BC1618 exposure also increased LC3 punctate counts (preserved by the lysosome inhibitor Bafilomycin A1) in stably expressing LC3-GFP HEK293 cells under glucose-rich growth conditions (Fig. 4E, F), suggesting that the compound itself is sufficient to induce autophagy.

BC1618 improves hepatic insulin sensitivity in HFD mice

We further evaluated BC1618 properties and drug potential. BC1618 *in vitro* testing demonstrated that BC1618 was metabolically stable in mouse and human hepatocytes and plasma (Supplementary Fig. 10). Investigative pharmacokinetic (pK) studies in mice indicated that BC1618 displayed excellent oral bioavailability with a peak of 2000 ng/ml within 0.5 h and 500 ng/ml in plasma at 4 h after an oral load of 20 mg/kg. In addition, BC1618 was well-tolerated in mice; tissue histology and clinical markers including creatinine, LDH, ALT, and creatine kinase activity were not altered compared to vehicle in a three-month toxicity study (Extended Data Fig. 6). Further evaluation of BC1618 toxicokinetic and off-targeting effects is currently under investigation.

Chronic low-grade inflammation is a defining character of metabolic diseases including NAFLD, insulin resistance, and T2D. Activated Ampk is essential in suppressing inflammation induced tissue injury, for example, through inhibiting LPS-induced inflammation [32], enhancing neutrophil chemotaxis and bacterial killing [33], and ameliorating vascular permeability, myocardial edema, and inflammation during sepsis [34]. These effects are in part due to the ability of activated Ampk to suppress NF-κB activity [35]. In THP1 cells stably expressing a NF-κB inducible luciferase reporter, BC1618 dose-dependently blocked LPS-induced luciferase activity (Extended Data Fig. 7A). BC1618 also attenuated LPS-induced cytokine release in human peripheral blood mononuclear cells (PBMC) (Extended Data Fig. 7B–C). We further examined BC1618 in LPS-induced acute lung inflammatory injury in mice. In response to LPS challenge, BC1618 dose-dependently attenuated mouse lung inflammation as indicated by lower BAL protein and cell counts, and lower levels of pro-inflammatory cytokines (Extended Data Fig. 8A–E). BC1618 treatment also alleviated the cell infiltration in LPS-challenged mouse lung tissues (Extended Data Fig. 8F). We also expanded the BC1618 efficacy study to other organs. Importantly, acute dosing of mice with BC1618 resulted in marked increase in phosphorylated Ampkα in liver, heart, and skeletal muscle compared with controls (Extended Data Fig. 9). Reduced Ampk activation is a pathogenic feature of obesity-associated metabolic disease, including insulin resistance and T2D [36]. Metformin exerts its beneficial metabolic affects primarily by suppressing hepatic glucose production and improving liver insulin sensitivity [37]. We

therefore evaluated the effects of BC1618 on insulin sensitivity in a diet-induced obese mouse model using the hyperinsulinemic euglycemic clamp. Body weight matched mice fed a high-fat diet for 20 weeks received an evening dose of vehicle or BC1618 prior to fasting and then a second dose 2 h prior to study. Plasma glucose levels were matched between groups during the hyperinsulinemic infusion and the glucose infusion rate (GIR) required to maintain euglycemia was assessed. In BC1618 treated mice, the GIR was approximately 2-fold greater than controls (Fig. 5A–B, P<0.001), indicating improved whole-body insulin sensitivity. There was no difference in whole-body glucose uptake or basal rates of hepatic glucose production between groups (Fig. 5C), however, insulin stimulated rates of hepatic glucose production were significantly reduced in BC1618 treated mice (Fig. 5D). This fully accounted for the differences in whole-body insulin sensitivity. Fasting plasma insulin levels were 2-fold less in BC1618 compared with vehicle treated mice, although the difference was not significant (Fig. 5E), and importantly plasma insulin levels were matched during the hyperinsulinemic infusion (Fig. 5E).

Discussion

Ampk, via binding to ADP/AMP, is a central regulator of energy homeostasis by coordinating metabolic pathways to balance nutrient supply with energy demands. Due to the known effects of Ampk activation on metabolism, Ampk has been targeted for therapeutic development to mitigate a range of human diseases including metabolic disorders and cancer [38]. So far, a wide array of compounds including metformin, phenformin, AICAR, A769662, 911, salicylate, and MT 63–78 have been shown to activate Ampk [39, 40]. Metformin, currently the first-line agent for type 2 diabetes treatment, activates Ampk through multiple mechanisms. As previously mentioned, metformin can inhibit the mitochondrial electron transporter chain (ETC) complex I activity to deplete ATP [41]. Metformin can also activate Ampk through pathways involving the lysosome [42]. Despite its wide clinical use, metformin administration has significant liabilities including the rare development of lactic acidosis and the common occurrence of gastrointestinal side effects [43]. In addition, metformin is not directly metabolized in either mice or humans, and thus requires transporters for enterocyte absorption, hepatocyte uptake, and renal epithelial cell elimination [44]. For patients with genetic deficiencies in these transporters, or in tissues where these transporters are poorly expressed, metformin has limited therapeutic benefit. As previously noted, pan-Ampk activator, such as Merck's MK-8722, improved glucose homeostasis but induced cardiac hypertrophy [8]. This cardiac hypertrophy is believed to be an on-target effect of enhancing myocardial Ampk activity. In our studies, BC1618 did not alter cardiac weight after two weeks of treatment in mice. This may reflect a difference between a constitutive allosteric activator and a compound such as BC1618 that only maintains pAmpk levels once physiologically activated.

The aldolase-mediated fructose-1,6-bisphosphate (FBP) sensing pathway has been recently proposed as another cellular regulator of Ampk that is independent of AMP [45]. This result increases the complexity of Ampk activation and renders an AMP mimetic or AMP/ADP based strategy as likely insufficient for full Ampk activation. Thus, there remains an unmet need for developing a new class of potent, specific, and well tolerated small molecule Ampk activators that function through mechanisms distinct from either allosteric Ampk activation

or modulating AMP/ADP levels. Interestingly, our findings indicate that Ampk activation is highly dependent on its reversible phosphorylation at Thr172, and this phosphorylation serves as a degron that binds to ubiquitin E3 ligase SCF[Fbxo48] for ubiquitylation and disposal. Thus, the mechanism for Ampk activation is intrinsically linked to the mechanism of Ampk inactivation. These observations differ from a recent report that cancer-specific MAGE-A3/6-TRIM28 ubiquitin ligase targets Ampkα for degradation [46]. Given that Ampk requires forming a heterotrimeric αβγ complex to be stable and active, alterations in a single component are unlikely to be significant regulators of overall in vivo activity. Enhancing the α subunit via inhibiting MAGE-A3/6-TRIM28 ligase is likely therefore to be insufficient to fully activate Ampk.

In summary, we have interrogated Fbxo48 structure to design, synthesize, and test a series of Fbxo48 small molecule inhibitors. Using an *in silico* approach, we identified a hit compound that potently activated Ampk *in vitro*, with 4 μM BC1583 exceeding the effects of 250 μM of AICAR. With further SAR studies, we synthesized a more potent, orally bioavailable, and metabolically stable Ampk activator, BC1618. Unlike metformin and AICAR that both trigger reduction of total Ampk protein (Supplementary Fig. 1, [47–49]), BC1618 effectively prevented pAmpkα from degradation and thereby preserved pAmpkα cellular protein levels. Target validation studies confirmed the interaction of the small molecule with Fbxo48 (Fig. 3C) and ineffectiveness of BC1618 in Fbxo48 knockdown cells (Fig. 3D). Ampk regulates numerous metabolic pathways including lipid synthesis and oxidation, glucose uptake and meabolism, mitochondrial biogenesis, autophagy, and protein synthesis. A recent study demonstrated that the Ampk regulatory β1 subunit stabilizing peptide ACIP ameliorated adipose tissue-wasting in a murine cancer cachexia model, with ACIP shielding against Ampkβ-interacting protein Cidea and preventing Ampkβ1 from degradation [50]. We show, by preserving the Ampk catalytic core and pAmpkα pool, BC1618 facilitates mitochondrial fission, inhibits the mTOR pathway, activates autophagy, and improves insulin sensitivity through inhibiting hepatic glucose production (Figs. 4, 5). Our study provides a platform for therapeutic development of a new genus of chemical entities that prolong Ampk activity and thus potentially target an array of conditions where dysregulated energy metabolism is a pathognomonic signature of the disease.

Material and Methods

Plasmids

F-box protein encoding plasmids were from our laboratory library described previously [51, 52]. Individual genes were inserted into a pcDNA3.1/V5-His TOPO vector (Invitrogen) to generate the C-terminal V5 and His tags. Human Ampkα2 cDNA was purchased from Dharmacon (Clone ID: 7262537). Ampkα2 WT plasmid was generated by inserting a PCR amplified fragment into a pcDNA3.1/V5-His TOPO vector. Ampkα2 point mutants were generated by site-directed mutagenesis with Ampkα2 WT in pcDNA3.1/V5-His TOPO as a template. Lkb1 *shRNA* (TRC Lentiviral Human STK11 *shRNA*) was purchased from Dharmacon.

Reagents and antibodies

The following antibodies were used: β-actin (A5441, Sigma), V5 (R960–25, ThermoFisher), Cul1 (sc-12761, Santa Cruz), Fbxo48 (orb183658, Biorbyt), and Mff (17090–1-AP, Protein Tech). The following antibodies were purchased from Cell Signaling Technologies: phospho-Ampkα Thr172 (#2535), Ampk α1/2 (#2532), Ampk β1/2 (#4150), Ubiquitin (#3936), Skp1 (#12248), phospho-ACC Ser79 (#11818), ACC (#3676), Lkb1 (#3047), PP2Cα (#3549), phospho-MFF Ser146 (#49281), phospho-Raptor Ser792 (#2083), Raptor (#2280), pS6 Ser235/236 (#4858), S6 (#2217), phospho-ULK1 Ser555 (#5869), ULK1 (#8054), LC3B (#2775). The following secondary antibodies were from Bio-Rad: goat anti-rabbit HRP (1706515), goat anti-mouse HRP (1706516). Cycloheximide (ALX-380–269-G005) was from Enzo Life Sciences. Leupeptin (L2884), AICAR (A9978) and metformin (PHR1084) were from Sigma. Bafilomycin A1 (88899–55-2), LDH cytotoxicity assay kits (601170), an alanine aminotransferase colorimetric activity assay kits (700260), and a creatinine (serum) colorimetric assay kit (700460) were from Cayman Chemical. MG132 (F1101) and the creatine kinase assay kit (50–489-260) were from Fisher Scientific. Protein DC assay kits were from Bio-Rad. QuikChange II XL site-directed mutagenesis kits (200522) were from Agilent. Mitotracker green FM (M7514), streptavidin magnetic beads (88816) and pcDNA3.1 directional TOPO expression kits (K490001) were from ThermoFisher Scientific. RNeasy plus mini kits (74134) were from Qiagen. Anti-Ubiquitin TUBEs (UM401) was from LifeSensors. ADP/ATP Ratio Bioluminescence Assay Kit was from BioVision. N-terminal biotin-labeled Ampkα (wild type, phopho-T172, T172D, T172A) peptides were from CHI Scientific. Purified human Fbxo48 protein (TP760375) was from Origene. Phosphorylated human Ampkα2/β2/γ1 (02–148) was from Carna Biosciences (Japan). All screen compounds (including BC1583 (**1**)) were from ChemDiv with >98% purity.

Cell lines

BEAS-2B cells were described in [53]. BEAS-2B cells were maintained in a 10 cm culture dish with HITES media supplemented with 10% FBS. Cells were subcultured to 6-well plates before treatment. After cell attachment (4 h), media were replaced with glucose free 2% DMEM media for overnight (16 h) treatment. Media were replaced with glucose free media the following day for 2–6 h treatment experiments. HepaRG cells were purchased from ThermoFisher Scientific. Cells were revived and maintained in William's E media containing thaw or maintenance medium supplements, respectively, according to the manufacturer's protocol. Before treatment, cells were seeded in 6-well plates with high glucose DMEM supplemented with 2% FBS for overnight incubation. Experiments were then performed on the following day. HEK293A cells stably expressing GFP-LC3 was purchased from Sigma. Cells were maintained in high glucose DMEM media supplemented with 10% FBS. Cells were split onto glass-bottom 35 mm plastic petri dishes (MatTek) pre-coated with collagen. After 6 h incubation, media were switched to high glucose 2% DMEM media with Bafilomycin A1 or BC1618 for additional 24 h incubation before DAPI staining. THP1-Lucia NF-κB cells stably expressing NF-κB inducible luciferase reporter were purchased from InvivoGen. Cells were maintained in RPMI 1640 media containing 2 mM Glutamine, 25 mM HEPES, 10% FBS with Pen-Strep and 100 μg/ml Zeocin.

Cell lysis

At indicated time points after changing to the media containing vehicle or drug, media were removed and cells were lysed in RIPA buffer supplemented with Pierce protease inhibitors (Thermo Scientific) without washing to preserve the pAmpkα signal. The RIPA buffer includes 20 mM Tris pH 7.5, 150 mM NaCl, 1% Triton X-100, freshly added protease inhibitor tablets. Lysates were kept on ice all the time. Total protein was normalized using a protein DC assay (BioRad) and lysates were resolved on 15 well 8% SDS-PAGE gels (Invitrogen, MOPS buffer) or 12% gels (MES buffer) for proteins smaller than 30 KDa.

Immunoprecipitation (IP)

For anti-ubiquitin TUBE pull down, cells were removed from media and lysed in 1% boiling SDS. Lysates were further boiled at 99°C with shaking for 10 min. Ice cold TBS supplemented with protease inhibitors, deubiquitylating enzyme inhibitors O-PA and PR-619 were added to lysate. The final SDS concentration decreased to 0.2%. Cells were sonicated and lysates were cleared at 18,000g for 10 min at 4°C. 800 μg total proteins were subjected to ubiquitin recognizing TUBE agarose pull down for 3 h at 4°C. TBS containing 0.1% Tween-20 were then used to wash beads for three times. SDS sample buffer was then added and boiled at 95°C for 5 min before protein immunoblot procedures. For V5 antibody-based IP, cells were lysed in cold PBS with 0.25% NP-40. 1.5 mg total proteins were used for 3 μg mouse V5 antibodies using IP. Protein elutates in SDS sample buffer were boiled and then resolved on 4–12% SDS-PAGE gels for Cul1, Skp1 and V5 protein immunoblot analysis.

In-cell pAMPK ELISA

BEAS-2B cells were plated in white 384-well plates (Thermo # 164610) in complete DMEM @ 7,500 cells/well and 293A cells were plated in poly-L-lysine-coated white 384-well plates (Thermo # 164610) in complete DMEM @ 15,000 cells/well. The plates were left at room temperature for 30–60 minutes before transferring to a TC incubator. The next day test compounds were prepared in glucose-free DMEM media with 2% FBS, L-Glut, P/S, HEPES. DMEM media with 4.5g/L glucose, 2% FBS, L-Glut, P/S, HEPES was included for determination of non-specific background signal. The growth media was removed from cells by flicking the plate upside-down a few times and blotting remaining liquid onto tissue paper. The cells were then washed in glucose-free DMEM media with 2% FBS, L-Glut, P/S, HEPES. This media was removed as described above. Immediately thereafter, 30 μL of compound solution was added using an Agilent Bravo liquid handler and the cells transferred to a TC incubator. The next day cells were fixed by adding an equal volume of pre-warmed 8% PFA/PBS and let sit for 30 min. The cells were washed 2x in TBS using a Biotek ELx405 automated washer. TBS was aspirated and cells permeabilized by adding 15 μL TBS/0.5% TX100, for 15 min. Cells were washed 3x in TBS containing 0.05% Tween-20 (TBS-T). TBS-T was aspirated, and cells were blocked by adding 15 μL TBS-T/1% BSA, for 15–60 min. The blocking solution was aspirated, and 15 μL primary antibody solution (pAMPKα (Cell Signaling, 40H9) 1:5,000 in TBS-T/1% BSA) was added. The plates were sealed and incubated at 4°C O/N or 2 hours at room temperature (RT). Next, the cells were washed 4x in TBS-T, TBS-T aspirated and 15 μL secondary antibody

solution added (αRabbit-HRP 1:20,000 (Invitrogen) in TBS-T/5% dry milk powder). Plates were sealed and incubated 1 hour at RT. The cells were then washed 4x in TBS-T, TBS-T aspirated and 25 μL of ECL reagent added. 20 minutes later luminescence was measured using a BMG ClarioStar microplate reader.

Homology Model

Fbxo48 protein sequence was first inputted in Discovery Studio 3.5 and a blast search was performed to identify the most homologous proteins. Next, from the blast search, the following proteins 3MKSB.dsv, 1NEXB.dsv, 2OVPB.dsv, 1P22A.dsv, 1T9RA.dsv were selected to construct the homology model using "Create Homology Models" function. Specific program parameters were: Protein optimize Sidechains: True, Waters: False, Cut overhangs: True, Refine Loops: True, Refine loops Optimization level: High, Refine loops Use DOPE method: True, Parallel Processing: True. The predicted models were then verified using "MODELER" function. The selected models were than further optimized using "Minimization" and "Refinement" function.

Mito Tracker staining

Final concentration of 100 nM Mito Tracker Green FM were added to cultured cells and incubated for 25 min at 37°C. Cells were then washed with 37°C serum free media with or without glucose for 4 times and maintained in 37°C culture chambers for confocal microscopy analysis.

DAPI staining

Cells were fixed with 4% paraformaldehyde in PBS at room temperature for 15 min. Cells were then washed in PBS at RT for 3 times before adding DAPI.

RNA sequencing

Total RNA from BEAS-2B cells was extracted using a RNeasy Plus Mini kit (Qiagen). Libraries were then prepared by Quick Biology (Pasadena, USA) using a KAPA Stranded RNA-Seq Kit. The workflow included mRNA enrichment, cDNA generation, and end repair to generate blunt ends, A-tailing, adaptor ligation, and PCR amplification. Different adaptors were used for multiplexing samples in one lane. Sequencing was performed on Illumina Hiseq3000/4000 for a pair end 150 run. Data quality check was done on Illumina SAV. Demultiplexing was performed with Illumina Bcl2fastq2 v 2.17 program. F-box protein mRNA levels in the glucose free treatment group were normalized to the high glucose media group.

Synthetic procedures

BC1618 synthesis—5 mmol of dibenzylamine (3) (Sigma, 98% purity) and 5 mmol of 2-([4-(trifluoromethyl) phenoxy]methyl) oxirane (4) (Sigma, 98% purity) were combined and stirred under N2 at 70°C for 24 h. The reaction was cooled down to produce the white crystal, which was then purified using column chromatography to obtain the final product as white powder (2.03 g, 86% yield). BC1618: 1H NMR (400 MHz, CDCl3) δ 7.51 (d, 2H), 7.31 (m, 8H), 7.25 (m, 3H), 6.88 (d, 2H), 4.10 (m, 1H), 3.89 (m, 2H), 3.75 (m, 2H), 3.55

(m, 2H), 2.68 (d, 2H), 1.55 (s, 1H); 13C NMR (DMSO, 300 MHz): δ 56.05, 58.56, 67.01, 71.01, 114.8, 120.61, 123.52, 125.67, 126.77, 128.08, 128.64, 139.24, 161.54. LCMS m/z 416.6 [M+H]+.

***In vitro* Fbxo48-pAmpkα binding assays**—Recombinant HIS-tagged Fbxo48 protein (1 μg) was prepared as bait via binding to Ni-NTA resin in PBS for 1 h. Fbxo48-HIS-NTA resin was then exposed to BC1618 with various concentrations before incubation with recombinant pAmpkα2/β2/γ1 complex for an additional 1h. Beads were then washed and proteins were eluted and immunoblotted.

***In vitro* protein-peptide binding assays**—pAmpkα peptide (Biotin-DGEFLRT(p)SCGSPN) (10 μg) was prepared as bait via binding to streptavidin agarose resin in PBS for 1 h. Recombinant Fbxo48 protein primed with BC1618 at various concentrations was captured by pAmpkα peptide resin for 1 h prior to elution and immunoblotting.

Cellular thermal shift assay (CETSA): 293T cells transfected with Fbxo48-V5 or Fbxo30-V5 were treated with control (DMSO) or BC1618 (3uM) for 30 min. Cells were then washed and equally fractioned into 10 aliquots and subjected to a range of increasing temperatures to promote protein denaturation. After a high-speed spin to precipitate heat-denatured proteins, the soluble protein fraction from each temperature was then immunoblotted for Fbxo48 or Fbxo30.

***In vitro* compound metabolic stability assays**—BC1618 (1 μM) was incubated in duplicate with liver microsomes or hepatocytes (BioReclamation IVT) at 37°C. The reaction contained microsomal protein in 100 mM potassium phosphate, 2 mM NADPH, 3 mM MgCl2, pH 7.4. A control reaction was performed for each test agent omitting NADPH to detect NADPH-free degradation. For plasma stability assays, BC1618 (5 μM) was incubated in duplicate with plasma at 37°C. At indicated times, an aliquot was removed from each experimental and control reaction and mixed with an equal volume of ice-cold stop solution (methanol containing propranolol as an internal analytical standard). Stopped reactions were kept on ice for at least 10 min and an additional volume of water was added. The samples were centrifuged to remove precipitated protein, and the supernatants were analyzed by LC-MS/MS to quantitate the remaining parent (Cyprotex). Data were converted to % remaining by dividing by the time zero concentration value. Data were fit to a first order decay model to determine half-life. Propantheline, Warfarin, Verapamil, Midazolam and Warfarin were used as reference compounds.

Quantitative Phosophoproteomics—Sample Preparation - BEAS-2B cells were treated either with BC1618 or vehicle control for 2 hours in 2% FBS DMEM without glucose. Cells were then washed with media and frozen in liquid nitrogen. Cells were scraped from the substrate in PBS, and lysis performed in 8M urea, 150mM NaCl, 50mM Tris, pH 8 with Roche PhosSTOP phosphatase inhibitor using a Next Advance Bullet Blender and 1mm silica beads. Lysate was incubated at room temperature for 1 hr with mixing, then clarified by centrifugation (10,000g for 10m). Protein lysates were reduced with 14 mM dithiothreitol for 30 min, followed by alkylation with 14 mM iodoacetamide for

45 min in the dark. Samples were then digested with trypsin at 37°C overnight, then cooled to room temperature and terminated with 5μL formic acid. Samples were then centrifuged 10,000g for 10m.

Solid Phase Extraction - Supernatant was then processed by solid phase extraction using an Empore C18 (3M) plate under vacuum. Columns were activated with 400μL 95/4.9/0.1 acetonitrile/water/TFA twice, then equilibrated with 400μL 0.1% TFA four times. Samples were loaded and then washed with 400 μL 0.1% TFA three times. Peptides were eluted with 200μL 70/29.9/0.1 acetonitrile/water/TFA twice and lyophilized.

Phosphopeptide Enrichment - Peptides were enriched using Titansphere TiO2 tips from GL sciences using the vendor protocol. Phosphopeptides were eluted using two eluents, 50μL 5% NH4OH and 50μL 5% pyrrolidine in water, then neutralized with 50% acetic acid, followed by lyophilization and reconstituted in 70 μL of 0.1% TFA.

Phosphopeptides were analyzed by nano LC-MS/MS with a Waters NanoAcquity HPLC system interfaced to a ThermoFisher Fusion Lumos mass spectrometer. Peptides were loaded on a trapping column and eluted over a 75μm analytical column at 350nL/min using a 2hr reverse phase gradient; both columns were packed with Jupiter Luna C18 resin (Phenomenex). The mass spectrometer was operated in data-dependent mode, with the Orbitrap operating at 60,000 FWHM and 15,000 FWHM for MS and MS/MS respectively. The instrument was run with a 3s cycle for MS and MS/MS. Advanced Precursor Determination was employed [54].

Summed phosphopeptide intensities corresponding to each detected phosphorylation site were filtered for only those phosphosites that were detected in all three replicates of at least one of the treatments, either vehicle or BC1618. Intensities were then log2-transformed and median normalized. Each remaining phosphosite was assigned a site group ID according to the assigned protein accession numbers and the corresponding modified amino acid. When multiple site group IDs matched, the one with more annotations in PTMsigDB was used [22]. For each phosphosite, a two-sample t-test was performed. The product of the resulting –log10 transformed P value and the sign of the difference in means was used to rank the phosphosites according to increased phosphorylation in BC1618 treated cells relative to vehicle treated cells. The resulting rank was prepared as a gct file and used as input for PTM-SEA, using the recommended parameters, with a minimum overlap of 8 PTMs [22].

Animal Studies—All procedures were approved by the University of Pittsburgh Institutional Animal Care and Use Committee (IACUC). The authors have complied with all relevant ethical regulations regarding animal use. For the PK study, C57BL/6 mice were randomized and given 1 dose of BC1618 (20 mg/kg) by oral gavage. Mice were then euthanized; plasma was isolated for BC1618 bioanalysis (Touchstone). For the toxicity study, C57BL/6 mice were given BC1618 in drinking water at 15 mg/kg/d (Low) and 30 mg/kg/d (High) doses for 3 months. Mice were then euthanized, and plasma samples were collected and assayed for markers of cytotoxicity. Alanine aminotransferase (ALT) activity, creatine kinase activity, lactate dehydrogenase (LDH) content, and creatinine content were measured following the manufacturer's protocol. Major organs were also collected and

processed for H&E staining. For hyperinsulinemic euglycemic clamp studies, diet-induced obese mice were purchased from Jackson Labs and allowed to acclimate at the University of Pittsburgh for two weeks prior to study. One week prior to study, mice underwent surgery to implant an indwelling catheter in the right jugular vein. The evening before the study (~5 PM), mice received an oral gavage of vehicle (40% PEG400) or BC1618 (20 mg/kg) and moved to new cages without access to food. The following morning, mice received a second dose of vehicle or drug (~6:30 AM) 2 h prior to starting the clamp study. Clamps were performed as previously described [55] with some modifications. Mice were infused with 3^{-3}H-glucose at a rate of 0.05 μCi/min for 120 min to determine basal glucose turnover. Next, a primed infusion of insulin and 3^{-3}H-glucose was administered at 10 mU·kg^{-1}·min^{-1} and 0.24 μCi/min, respectively, for 3 min, after which rates were reduced to 3 mU·kg^{-1}·min^{-1} insulin and 0.1 μCi/min 3^{-3}H-glucose for the remainder of the experiment. Blood was collected via tail massage for plasma glucose, insulin and tracer levels at 10 min intervals during the 120 min infusion and a variable infusion of 20% dextrose was given to maintain euglycemia. Glucose turnover was calculated as the ratio of the 3^{-3}H-glucose infusion rate to the specific activity of plasma glucose at the end of the basal infusion and during the last 40 min of the hyperinsulinemic infusion. Hepatic glucose output represents the difference between the glucose infusion rate and the rate of glucose appearance. Following collection of the final blood sample, mice were anesthetized with an intravenous injection of 150 mg/kg pentobarbital and tissues were harvested and froze with aluminum forceps in liquid nitrogen. All tissues were stored at −80°C until later use.

Human Tissue—Frozen livers from explanted or resected livers with NASH or normal human livers (without hepatitis) collected at the time of resection of metastasis to the liver from deidentified patients were obtained from the Health Sciences Tissue Bank, University of Pittsburgh, under an approved IRB (Exempt) protocol. These tissues were used for protein isolation and immunoblot analysis as described previously.

Quantification and statistical analysis—Protein Signal densitometry was quantified via ImageJ. Results in this study are expressed as means ± SEM of independent experiments, and measurements were taken from distinct samples. Group comparisons were performed using two-tailed unpaired Student's *t* test, one-way ANOVA with multiple comparisons, or as noted. *P*<0.05 was considered statistically significant. All statistical analyses were carried out using the Graph Pad Prism 6.0 program.

Reporting Summary—Further information on research design is available in the Nature Research Reporting Summary linked to this article.

Data Availability—All relevant data are available from the authors and/or included in the manuscript or Supplementary Information. The data that support the findings of this study are available from the corresponding author upon reasonable request. Phospho-proteomics data can be accessed at MassIVE database under ID: MSV000086334.
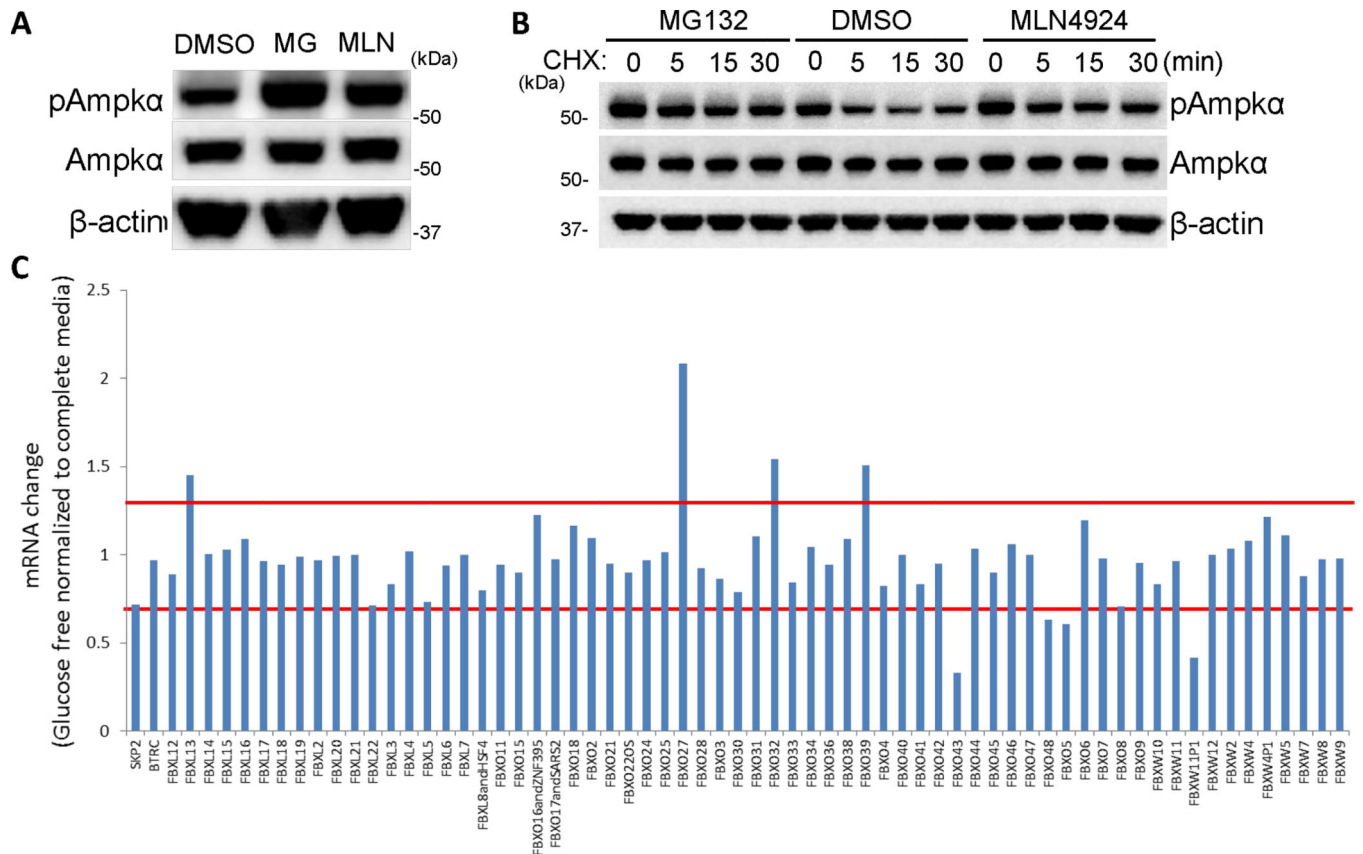
Extended Data
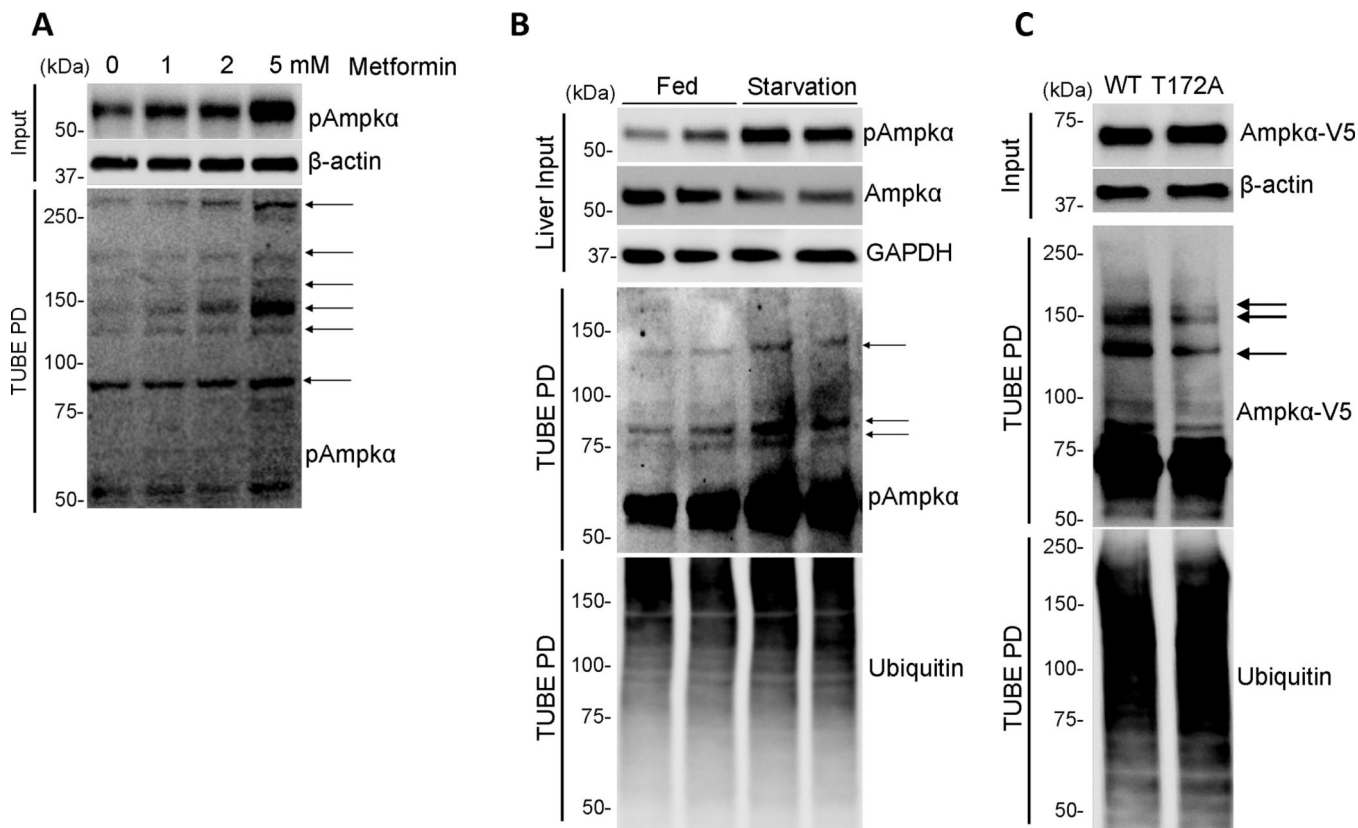
Extended Data Fig. 1. pAmpkα undergoes ubiquitin proteasomal degradation.
(A) BEAS-2B cells were pretreated in glucose free media with increasing concentrations of metformin for 4h. Whole cell extracts were subjected to TUBE agarose beads pull downs (PD) and immunoblotting (Results are representative of three independent experiments).
(B) Fed and overnight starved mouse liver extracts were subjected to TUBE agarose beads pull down (PD) and immunoblotting (Results are representative of three independent experiments). **(C)** BEAS-2B cells were transfected with either WT or T172A mutant Ampk. Whole cell extracts were subjected to TUBE agarose beads pull down (PD) and immunoblotting. Arrows indicate polyubiquitylated products in each blot (Results are representative of three independent experiments).

Extended Data Fig. 2. pAmpkα ubiquitylation and degradation is mediated by an F-box protein.

(A) BEAS-2B cells were incubated in glucose free 2% DMEM media containing DMSO, MG132 (20 μM, MG) or MLN4924 (5 μM) for 1.5 h. Cells were then collected for immunoblotting (Results are representative of two independent experiments).

(B) BEAS-2B cells were preincubated in glucose free 2% DMEM media containing DMSO, MG132 (20 μM) or MLN4924 (5 μM) for 1 h. CHX (40 μg/ml) was then added at indicated time points. Cells were collected at same time for immunoblotting (Results are representative of two independent experiments).

(C) BEAS-2B cells were incubated in high glucose then switched to glucose free 2% DMEM media for 16 h. Total RNA were purified using Qiagen RNeasy Plus Mini Kit. RNA sequencing was then performed by the Quick Biology commercial service. Differentially expressed genes of F-box protein families were plotted and 30% expression level difference was indicated in the red line cut off (Data are the mean of two biological replicates).

Extended Data Fig. 3. Screening of F-box proteins involved in pAmpkα degradation.
(A) BEAS-2B cells were nucleofected with a series of V5 tagged F-box protein encoding plasmids (3 μg). After incubation for 48 h, high glucose media was switched to glucose free 2% FBS DMEM media for 1 h. Cells were then collected for immunoblotting (Results are representative of two independent experiments).
(B, C) BEAS-2B cells were nucleofected with increasing amounts of either *Skp2*-V5 or *Fbxl5*-V5 plasmids. After incubation for 48 h, growth media were changed to glucose free media for 1 h before immunoblotting (Results are representative of two independent experiments). NS indicates a non-specific band.
(D). In vitro ubiquitinylation of Ampk. Recombinant ubiquitin E1, E2 conjugating enzymes and ubiquitin was incubated with or without Fbxo48 with pAmpk and polyubiquitinylated

products were detected on immunoblots (arrows) (Results are representative of two independent experiments).
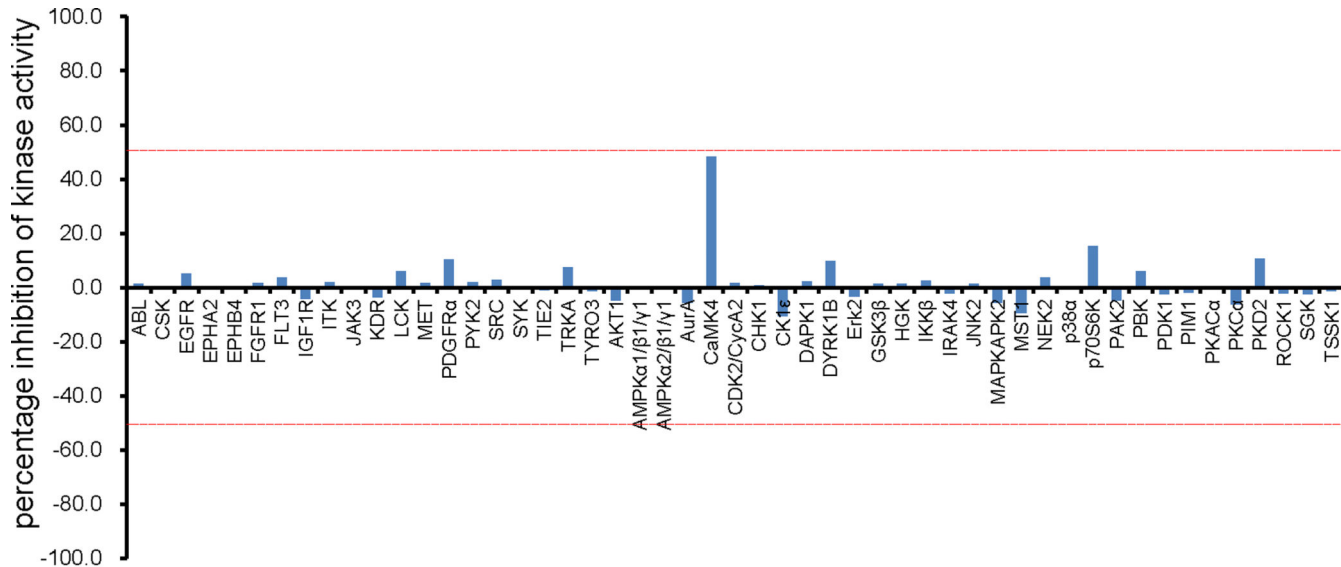
Target kinase

ABL, CSK, EGFR, EPHA2, EPHB4, FGFR1, FLT3, IGF1R, ITK, JAK3, KDR, LCK, MET, PDGFRα, PYK2, SRC, SYK, TIE2, TRKA, TYRO3, AKT1, AMPKα1/β1/γ1, AMPKα2/β1/γ1, AurA, CaMK4, CDK2/CycA2, CHK1, CK1ε, DAPK1, DYRK1B, Erk2, GSK3β, HGK, IKKβ, IRAK4, JNK2, MAPKAPK2, MST1, NEK2, p38α, p70S6K, PAK2, PBK, PDK1, PIM1, PKACα, PKCα, PKD2, ROCK1, SGK, TSSK1

BC1618: 10 μM

Extended Data Fig. 4. BC1618 off-targeting kinase screen
The inhibitory activities for BC1618 (10 μM) against 51 kinases (ABL, CSK, EGFR, EPHA2, EPHB4, FGFR1, FLT3, IGF1R, ITK, JAK3, KDR, LCK, MET, PDGFRα, PYK2, SRC, SYK, TIE2, TRKA, TYRO3, AKT1, AMPKα1/β1/γ1, AMPKα2/β1/γ1, AurA, CaMK4, CDK2/CycA2, CHK1, CK1ε, DAPK1, DYRK1B, Erk2, GSK3β, HGK, IKKβ, IRAK4, JNK2, MAPKAPK2, MST1, NEK2, p38α, p70S6K, PAK2, PBK, PDK1, PIM1, PKACα, PKCα, PKD2, ROCK1, SGK, TSSK1) were measured and percentage inhibition of kinase activity was plotted. 50% change of kinase activities is indicated by a red line cut off line (CarnaBio) (Data are the mean of two biological replicates).
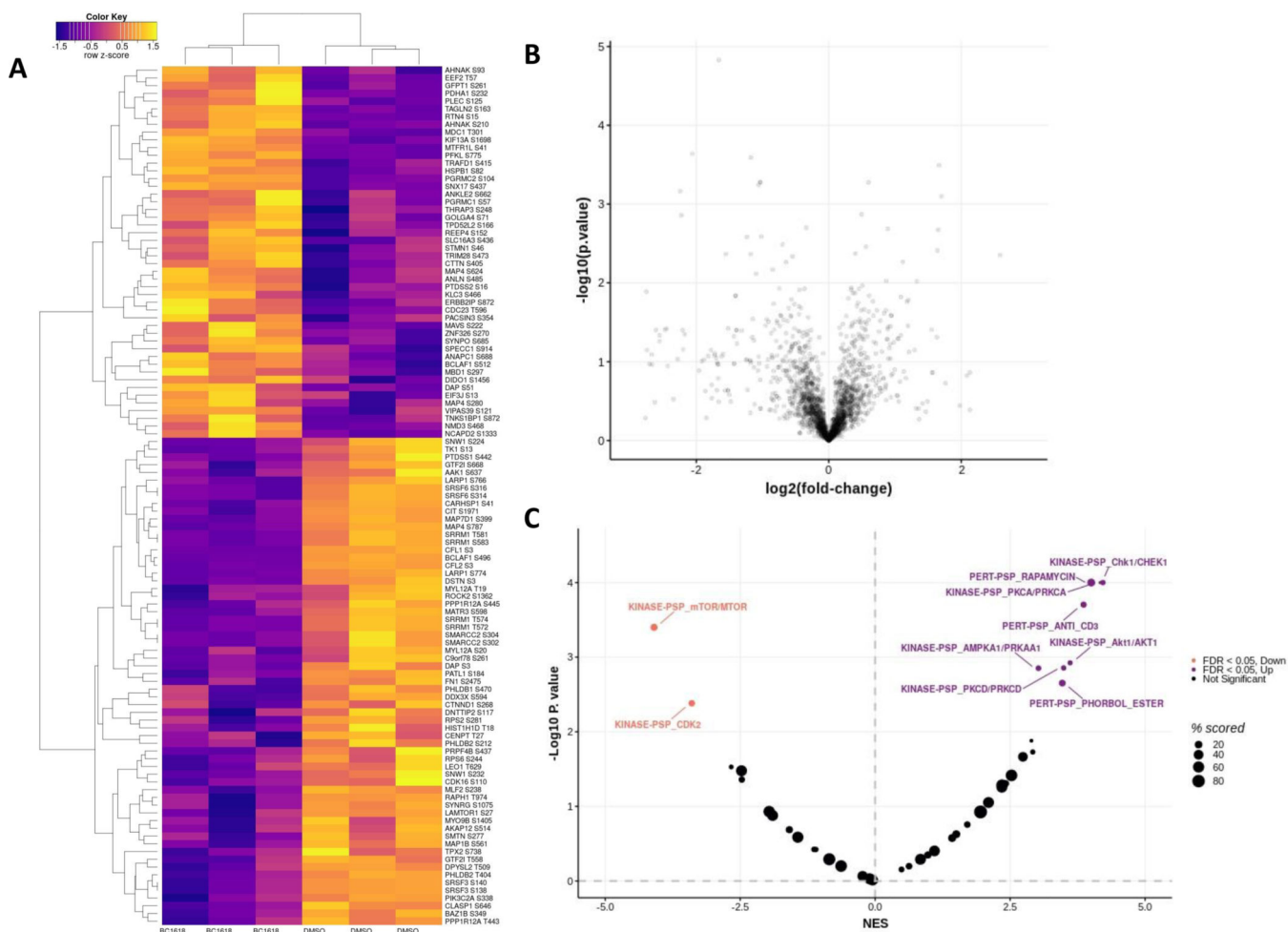
Extended Data Fig. 5. PTM-SEA analysis of BC1618 phosphoproteome.

(A) BEAS-2B cells were treated with BC1618 (3μM) or vehicle control and the alterations in the phosphoproteome were assessed using mass spectrometry. Heatmap of those phosphosites with p<0.05 (t-test) comparing BC1618 (left side) to DMSO control (right). Color indicates log2 normalized intensity values as row z-score. Row names indicate the corresponding protein and phosphorylation site.

(B) Volcano plot of statistical significance (-log10 p. value, y-axis) and the effect size (log2 scaled fold-change, x-axis) of BC1618 treated cells compared to DMSO control, where positive values represent phosphosites higher in BC1618 treated cells.

(C) Volcano plot of enrichment of various phosphoproteome signatures. The x axis indicates the normalized enrichment score (NES) between BC1618 and DMSO control, with positive values indicating shared phosphosite signatures and negative values indicating opposed phosphosite signatures. Dot size indicates the percent overlap of phosphosites associated with the signature and experimentally assayed phosphosites. Red indicates significantly upregulated signatures while green indicates significantly downregulated signatures (permutation-based FDR < 0.05). Grey indicates non-significant signatures (Data are from three biological replicates).
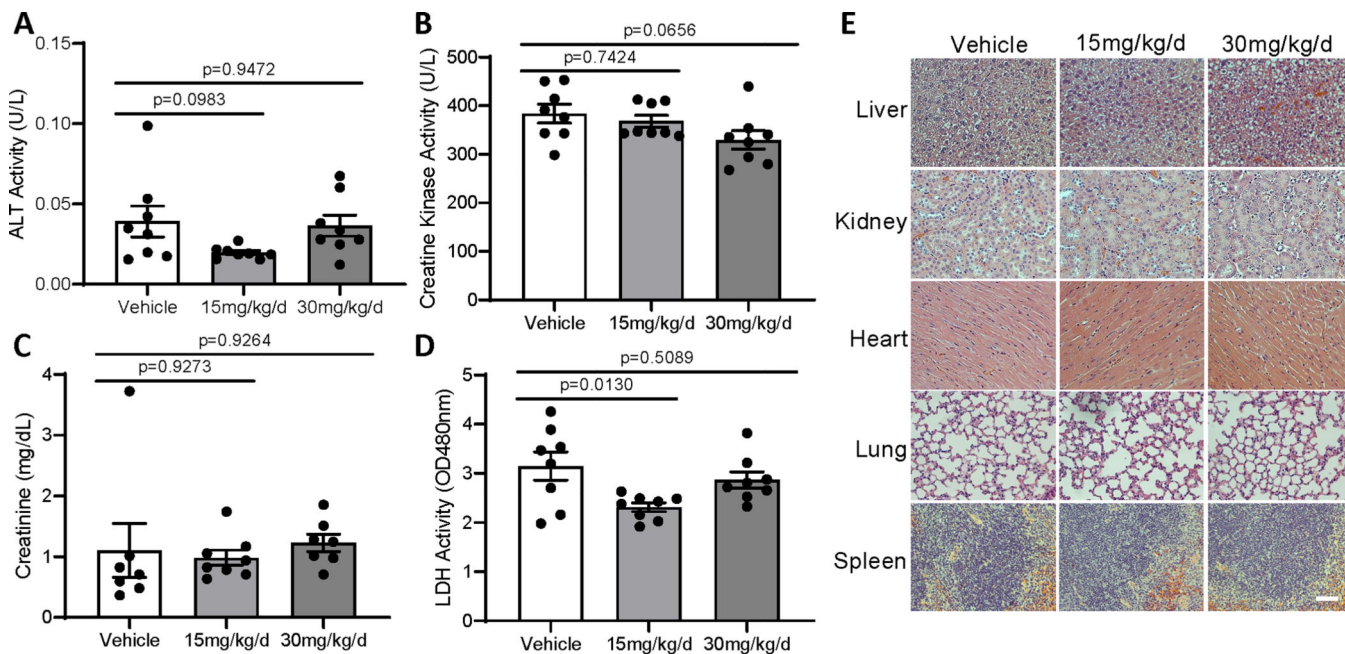
**Extended Data Fig. 6. BC1618 in vivo toxicity studies**
(A-D) C57BL/6 mice were given BC1618 in drinking water at 15 mg/kg/d (low) and 30 mg/kg/d (high) doses for 3 months. Mice were then euthanized, and plasma samples were collected and assayed for markers of cytotoxicity. Alanine aminotransferase (ALT) activity, creatine kinase activity, lactate dehydrogenase (LDH) content, and creatinine content were measured following the manufacturer's protocol. **(E)** Major organs were collected and processed for H&E staining; scale bar: 100 μm. Data represented mean +/− SEM. Data points represent n=7–8 independent mice per group, and p-values are indicated, as calculated by one-way ANOVA with Dunnett's test of multiple comparisons (A-D).
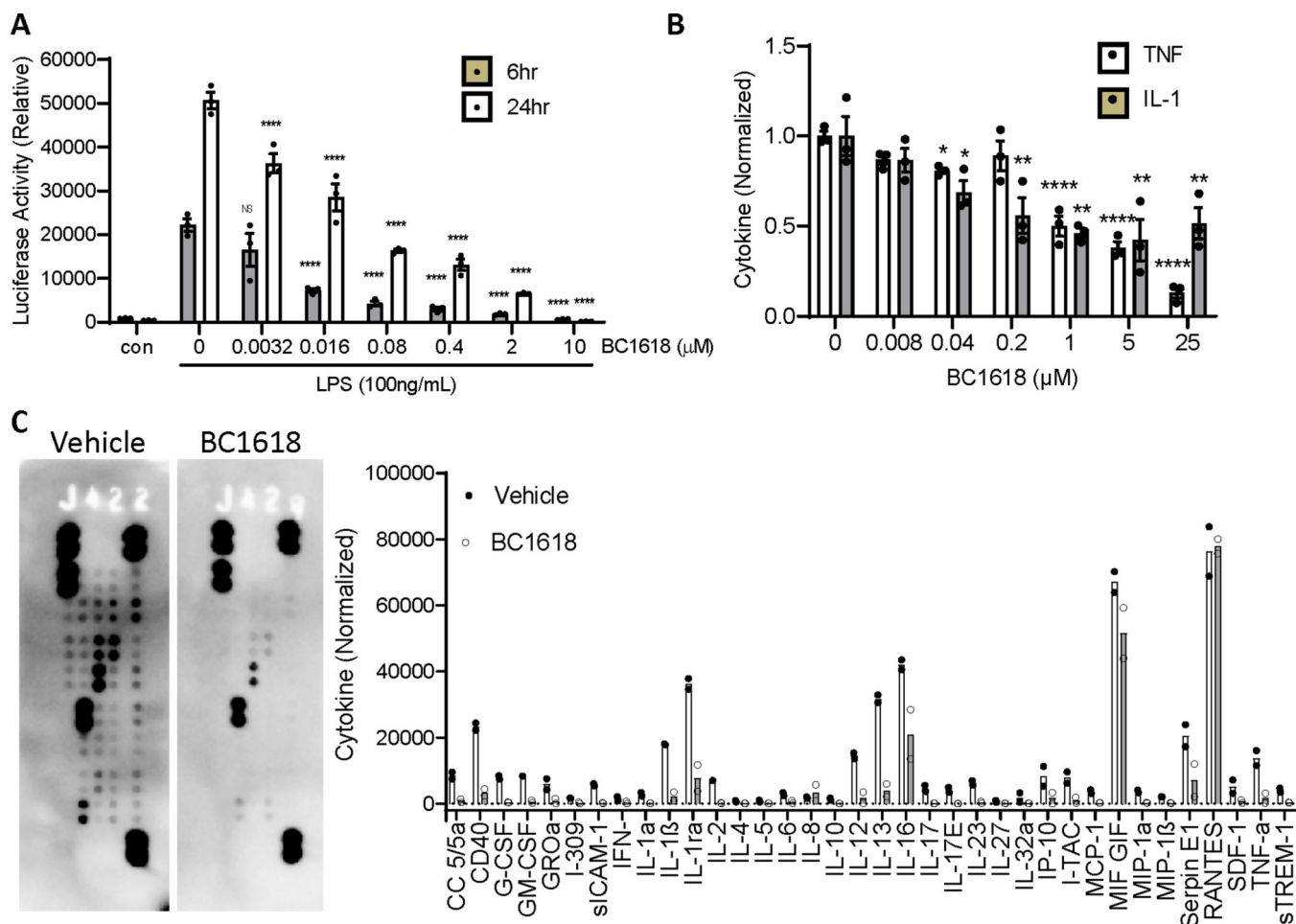
**Extended Data Fig. 7. BC1618 is anti-inflammatory in vitro.**

(A) THP1 cells stably expressing an NF-κB inducible luciferase (secretary) reporter were treated with LPS (100 ng/ml) and BC1618 at indicated concentrations for 6 h or 24 h before supernatant was collected for luciferase activity assay following the manufacturer's protocol. Data are shown as the mean ± SEM of three independent biological replicates, and significance was measured by one-way ANOVA with Dunnett's test of multiple comparisons relative to 0μM BC1618+LPS. For 6hs, 0.0032μM: p=0.0868; for 0.016,0.08, 0.4, 2, and 10μM: p<0.0001. For 24hr, 0.0032μM: p=0.0002; for 0.016,0.08, 0.4, 2, and 10μM: p<0.0001. **(B)** 50K PBMC cells were cultured in 96 well plates before being exposed to BC1618 at indicated concentrations for 18 h. Cells were then treated with LPS (10 ng/ml) for an additional 4 h. Media were then collected and TNF and IL-1 concentration were determined by ELISA. Data are shown as the mean ± SEM of three independent biological replicates, and significance was measured by one-way ANOVA with Dunnett's test of multiple comparisons relative to 0μM BC1618 for both cytokines. For TNF treatment, 0.008μM: p=0.2212; 0.04μM: p=0.0375; 0.2μM: p=0.3585; for 1, 5, and 25μM: p<0.0001. For IL-1 treatment, 0.008μM: p=0.7497; 0.04μM: p=0.0919; 0.2μM: p=0.0126; 1μM: p=0.0028; 5μM: p=0.0015; 25μM: p=0.0065. Significance is also indicated as follows: *, P <0.05; **, P < 0.01; ***, P <0.001; ****, P<0.0001 **(C)** PBMC cells (1 mL at 1.0×10^6/ml) were treated with BC1618 (5 μM) for 18 h. Cells were then treated with 100 ng/ml

LPS for additional 4 h. Cytokine release was monitored by the human cytokine array (R&D systems). The results from a cytokine array dot blot are shown and quantitated (Data are shown as the mean of two independent biological replicates).
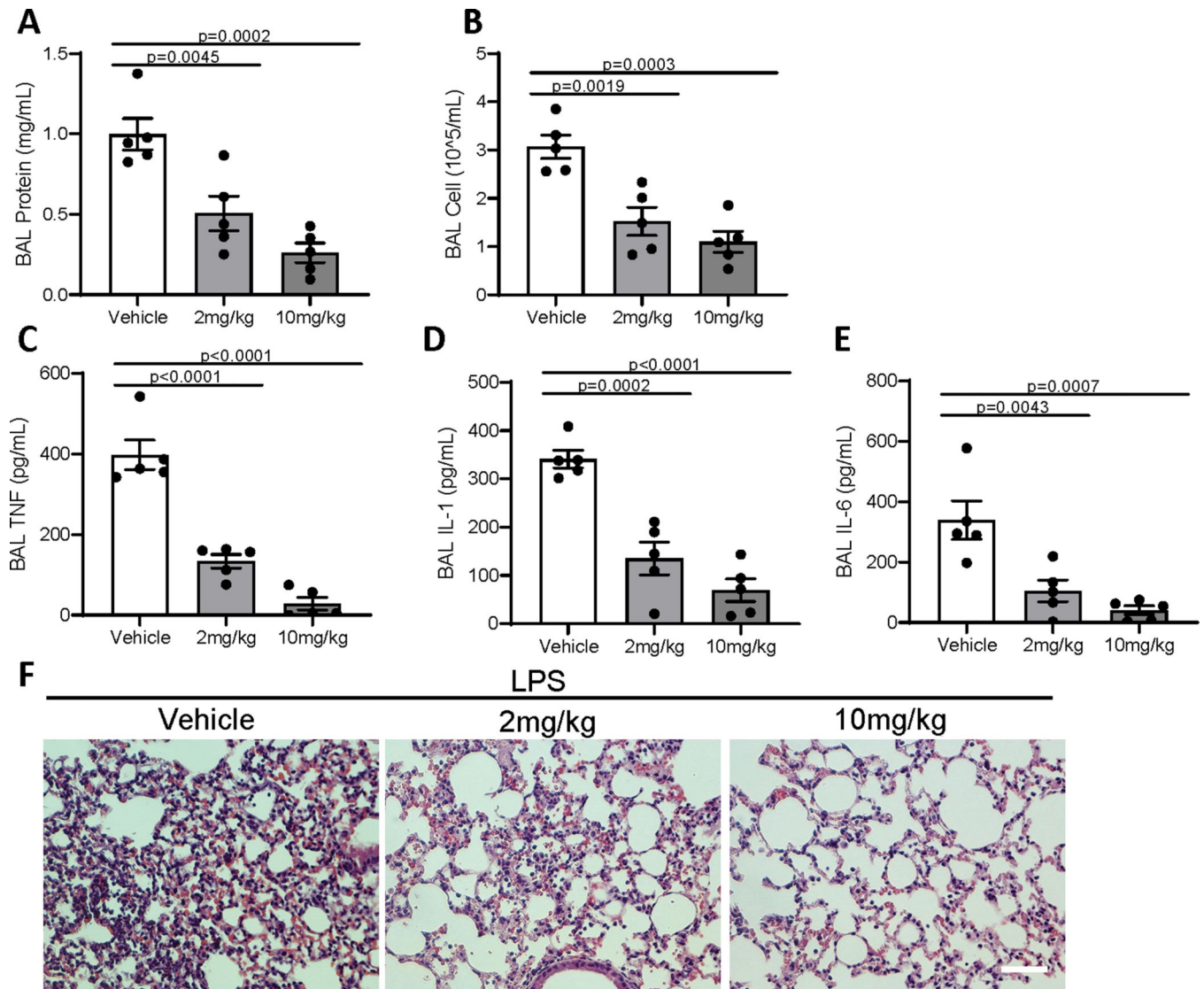
Extended Data Fig. 8. BC1618 reduces lung inflammation in endotoxin treated mice.
C57BL/6 mice were administered i.p. with vehicle, 2 or 10 mg/kg of BC1618. Mice were then immediately challenged with LPS (3 mg/kg) for an additional 18 h. Mice were euthanized and lungs were lavaged with saline, harvested, and then homogenized. Bronchoalveolar lavage (BAL) protein **(A)**, cell counts **(B)** and cytokines **(C-E)** were measured. **(F)** Representative mouse lung tissue H&E staining; scale bar: 100 μm. Data represented mean +/− SEM (n=5 independent mice per group). P-values are indicated as calculated by one-way ANOVA with Dunnett's test of multiple comparisons (A-E).
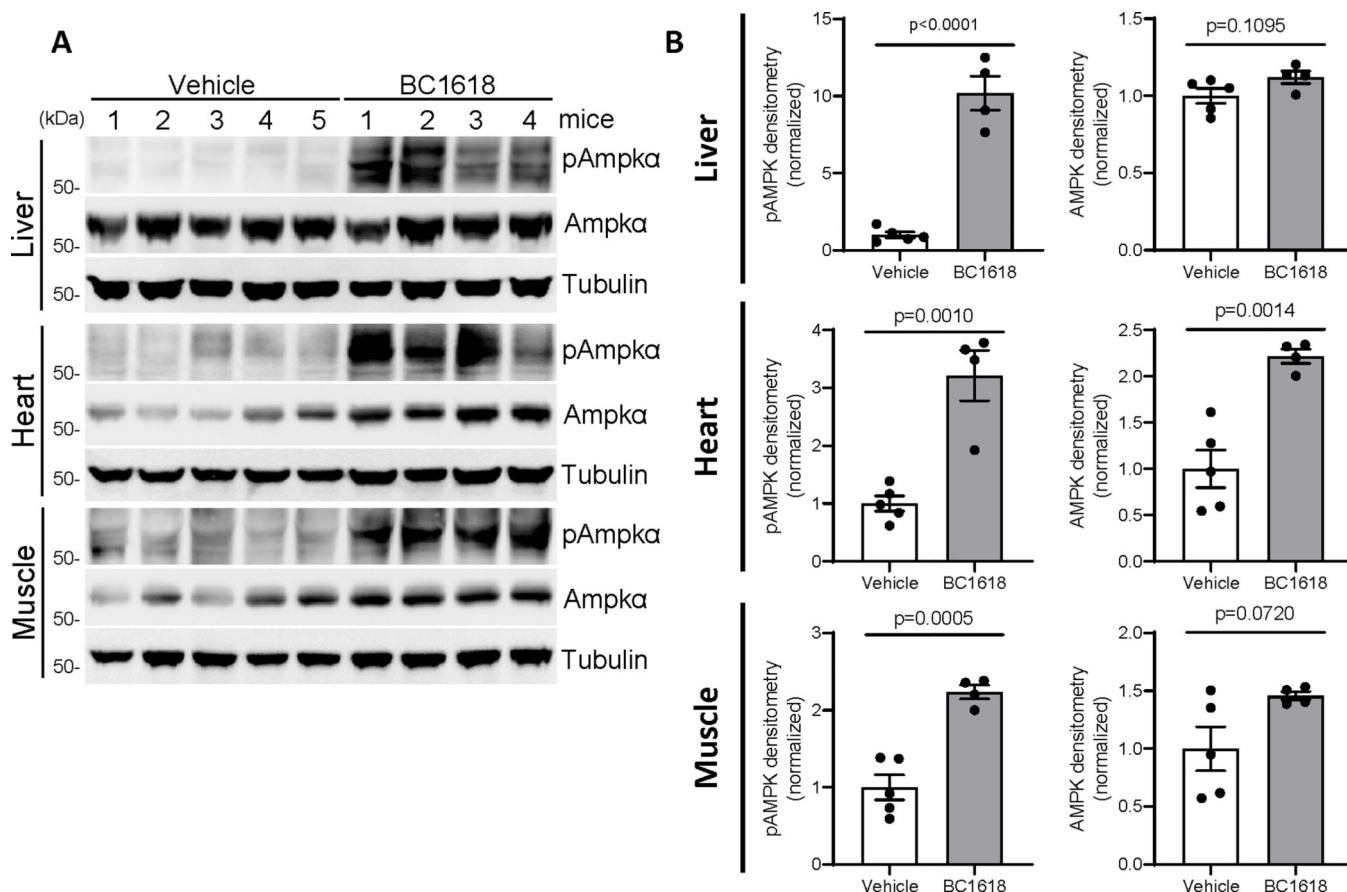
Extended Data Fig. 9. BC1618 increases Ampkα protein levels in mice after dietary restriction.
(A, B) C57BL/6 mice were intraperitoneally (i.p.) administered with vehicle or BC1618 (20 mg/kg) on day 1 and simultaneously chow was removed for overnight starvation. After a 17 h fast, mice were given vehicle or BC1618 i.p. 30 min later, mice were euthanized, PBS was perfused through heart to remove blood. Heart, liver, and skeletal muscle was collected and fresh frozen for tissue homogenization and immunoblotting. The pAmpkα and Ampkα protein levels were quantitated and plotted in **B.** Densitometry data were corrected to tubulin and normalized to vehicle. Data represented mean +/− SEM (n=4–5 independent mice per group). P-values are indicated as calculated by two-tailed unpaired t-test (B).

Supplementary Material

Refer to Web version on PubMed Central for supplementary material.

Acknowledgments

References

1. Hardie DG, Ross FA, and Hawley SA, AMPK: a nutrient and energy sensor that maintains energy homeostasis. Nat Rev Mol Cell Biol, 2012. 13(4): p. 251–262. [PubMed: 22436748]

2. Mihaylova MM and Shaw RJ, The AMPK signalling pathway coordinates cell growth, autophagy and metabolism. Nat Cell Biol, 2011. 13(9): p. 1016–1023. [PubMed: 21892142]

3. Hardie DG, AMPK: positive and negative regulation, and its role in whole-body energy homeostasis. Curr Opin Cell Biol, 2015. 33: p. 1–7. [PubMed: 25259783]

4. Kim J, et al. , AMPK activators: mechanisms of action and physiological activities. Exp Mol Med, 2016. 48: p. e224. [PubMed: 27034026]

5. Sanders MJ, et al. , Investigating the mechanism for AMP activation of the AMP-activated protein kinase cascade. Biochem J, 2007. 403(1): p. 139–48. [PubMed: 17147517]

6. Herzig S. and Shaw RJ, AMPK: guardian of metabolism and mitochondrial homeostasis. Nat Rev Mol Cell Biol, 2018. 19(2): p. 121–135. [PubMed: 28974774]

7. Cool B, et al. , Identification and characterization of a small molecule AMPK activator that treats key components of type 2 diabetes and the metabolic syndrome. Cell Metab, 2006. 3(6): p. 403–16. [PubMed: 16753576]

8. Myers RW, et al. , Systemic pan-AMPK activator MK-8722 improves glucose homeostasis but induces cardiac hypertrophy. Science, 2017.

9. Carling D, AMPK signalling in health and disease. Curr Opin Cell Biol, 2017. 45: p. 31–37. [PubMed: 28232179]

10. Steneberg P, et al. , PAN-AMPK activator O304 improves glucose homeostasis and microvascular perfusion in mice and type 2 diabetes patients. JCI Insight, 2018. 3(12).

11. Zhou G, et al. , Role of AMP-activated protein kinase in mechanism of metformin action. Journal of Clinical Investigation, 2001. 108(8): p. 1167–1174.

12. Hawley SA, et al. , Complexes between the LKB1 tumor suppressor, STRADα/β and MO25α/β are upstream kinases in the AMP-activated protein kinase cascade. Journal of Biology, 2003. 2(4): p. 28. [PubMed: 14511394]

13. Shaw RJ, et al. , The tumor suppressor LKB1 kinase directly activates AMP-activated kinase and regulates apoptosis in response to energy stress. Proc Natl Acad Sci U S A, 2004. 101(10): p. 3329–35. [PubMed: 14985505]

14. Deshaies RJ and Joazeiro CA, RING domain E3 ubiquitin ligases. Annu Rev Biochem, 2009. 78: p. 399–434. [PubMed: 19489725]

15. Xiu X, et al. , Genetic analysis of the FBXO48 gene in Chinese Han patients with Parkinson disease. Neurosci Lett, 2013. 541: p. 224–6. [PubMed: 23485738]

16. Smith BK, et al. , Treatment of nonalcoholic fatty liver disease: role of AMPK. Am J Physiol Endocrinol Metab, 2016. 311(4): p. E730–e740. [PubMed: 27577854]

17. Corton JM, et al. , 5-aminoimidazole-4-carboxamide ribonucleoside. A specific method for activating AMP-activated protein kinase in intact cells? Eur J Biochem, 1995. 229(2): p. 558–65. [PubMed: 7744080]

18. Fullerton MD, et al. , Single phosphorylation sites in Acc1 and Acc2 regulate lipid homeostasis and the insulin-sensitizing effects of metformin. Nat Med, 2013. 19(12): p. 1649–1654. [PubMed: 24185692]

19. Jafari R, et al. , The cellular thermal shift assay for evaluating drug target interactions in cells. Nat Protoc, 2014. 9(9): p. 2100–22. [PubMed: 25101824]

20. Sengupta S, et al. , Discovery of NV-5138, the first selective Brain mTORC1 activator. Sci Rep, 2019. 9(1): p. 4107. [PubMed: 30858438]

21. Chen Y, et al. , A small molecule NRF2 activator BC-1901S ameliorates inflammation through DCAF1/NRF2 axis. Redox Biol, 2020. 32: p. 101485. [PubMed: 32171724]

22. Krug K, et al. , A Curated Resource for Phosphosite-specific Signature Analysis. Mol Cell Proteomics, 2019. 18(3): p. 576–593. [PubMed: 30563849]

23. Gwinn DM, et al. , AMPK phosphorylation of raptor mediates a metabolic checkpoint. Mol Cell, 2008. 30(2): p. 214–26. [PubMed: 18439900]

24. Chang TW, et al. , Does OKT3 monoclonal antibody react with an antigen-recognition structure on human T cells? Proc Natl Acad Sci U S A, 1981. 78(3): p. 1805–8. [PubMed: 6165018]

25. Tamas P, et al. , Regulation of the energy sensor AMP-activated protein kinase by antigen receptor and Ca2+ in T lymphocytes. J Exp Med, 2006. 203(7): p. 1665–70. [PubMed: 16818670]

26. Zogovic N, et al. , Coordinated activation of AMP-activated protein kinase, extracellular signal-regulated kinase, and autophagy regulates phorbol myristate acetate-induced differentiation of SH-SY5Y neuroblastoma cells. J Neurochem, 2015. 133(2): p. 223–32. [PubMed: 25348263]

27. Toyama EQ, et al. , AMP-activated protein kinase mediates mitochondrial fission in response to energy stress. Science, 2016. 351(6270): p. 275–281. [PubMed: 26816379]

28. Egan DF, et al. , Phosphorylation of ULK1 (hATG1) by AMP-activated protein kinase connects energy sensing to mitophagy. Science, 2011. 331(6016): p. 456–61. [PubMed: 21205641]

29. Kim J, et al. , AMPK and mTOR regulate autophagy through direct phosphorylation of Ulk1. Nat Cell Biol, 2011. 13(2): p. 132–41. [PubMed: 21258367]

30. Egan DF, et al. , Phosphorylation of ULK1 (hATG1) by AMP-activated protein kinase connects energy sensing to mitophagy. Science (New York, N.Y.), 2011. 331(6016): p. 456–461.

31. Mizushima N. and Yoshimori T, How to interpret LC3 immunoblotting. Autophagy, 2007. 3(6): p. 542–5. [PubMed: 17611390]

32. Hoogendijk AJ, et al. , AMP-activated protein kinase activation by 5-aminoimidazole-4-carbox-amide-1-beta-D-ribofuranoside (AICAR) reduces lipoteichoic acid-induced lung inflammation. J Biol Chem, 2013. 288(10): p. 7047–52. [PubMed: 23322781]

33. Park DW, et al. , Activation of AMPK enhances neutrophil chemotaxis and bacterial killing. Mol Med, 2013. 19: p. 387–98. [PubMed: 24091934]

34. Castanares-Zapatero D, et al. , Connection between cardiac vascular permeability, myocardial edema, and inflammation during sepsis: role of the alpha1AMP-activated protein kinase isoform. Crit Care Med, 2013. 41(12): p. e411–22. [PubMed: 23963133]

35. Salminen A, Hyttinen JMT, and Kaarniranta K, AMP-activated protein kinase inhibits NF-κB signaling and inflammation: impact on healthspan and lifespan. Journal of Molecular Medicine (Berlin, Germany), 2011. 89(7): p. 667–676.

36. Ruderman NB, et al. , AMPK, insulin resistance, and the metabolic syndrome. J Clin Invest, 2013. 123(7): p. 2764–72. [PubMed: 23863634]

37. Viollet B, et al. , Cellular and molecular mechanisms of metformin: an overview. Clin Sci (Lond), 2012. 122(6): p. 253–70. [PubMed: 22117616]

38. Grahame Hardie D, Regulation of AMP-activated protein kinase by natural and synthetic activators. Acta Pharmaceutica Sinica B, 2016. 6(1): p. 1–19. [PubMed: 26904394]

39. Xiao B, et al. , Structural basis of AMPK regulation by small molecule activators. Nat Commun, 2013. 4: p. 3017. [PubMed: 24352254]

40. Hawley SA, et al. , The ancient drug salicylate directly activates AMP-activated protein kinase. Science, 2012. 336(6083): p. 918–22. [PubMed: 22517326]

41. Owen MR, Doran E, and Halestrap AP, Evidence that metformin exerts its anti-diabetic effects through inhibition of complex 1 of the mitochondrial respiratory chain. Biochem J, 2000. 348 Pt 3: p. 607–14. [PubMed: 10839993]

42. Zhang CS, et al. , Metformin Activates AMPK through the Lysosomal Pathway. Cell Metab, 2016. 24(4): p. 521–522. [PubMed: 27732831]

43. Type 2 diabetes and metformin. First choice for monotherapy: weak evidence of efficacy but well-known and acceptable adverse effects. Prescrire Int, 2014. 23(154): p. 269–72. [PubMed: 25954799]

44. Chen W, et al. , The ubiquitin E3 ligase SCF-FBXO24 recognizes deacetylated nucleoside diphosphate kinase A to enhance its degradation. Mol Cell Biol, 2015. 35(6): p. 1001–13. [PubMed: 25582197]

45. Zhang CS, et al. , Fructose-1,6-bisphosphate and aldolase mediate glucose sensing by AMPK. Nature, 2017. 548(7665): p. 112–116. [PubMed: 28723898]

46. Pineda CT, et al. , Degradation of AMPK by a cancer-specific ubiquitin ligase. Cell, 2015. 160(4): p. 715–28. [PubMed: 25679763]

47. Vlotides G, et al. , Anticancer effects of metformin on neuroendocrine tumor cells in vitro. Hormones (Athens), 2014. 13(4): p. 498–508. [PubMed: 25402373]

48. Groenendijk FH, et al. , Sorafenib synergizes with metformin in NSCLC through AMPK pathway activation. Int J Cancer, 2015. 136(6): p. 1434–44. [PubMed: 25080865]

49. Ducommun S, et al. , Enhanced activation of cellular AMPK by dual-small molecule treatment: AICAR and A769662. Am J Physiol Endocrinol Metab, 2014. 306(6): p. E688–96. [PubMed: 24425763]

50. Rohm M, et al. , An AMP-activated protein kinase-stabilizing peptide ameliorates adipose tissue wasting in cancer cachexia in mice. Nat Med, 2016. 22(10): p. 1120–1130. [PubMed: 27571348]

Methods References:

51. Chen BB, et al. , Skp-cullin-F box E3 ligase component FBXL2 ubiquitinates Aurora B to inhibit tumorigenesis. Cell Death Dis, 2013. 4: p. e759. [PubMed: 23928698]

52. Chen BB, et al. , F-box protein FBXL2 targets cyclin D2 for ubiquitination and degradation to inhibit leukemic cell proliferation. Blood, 2012. 119(13): p. 3132–41. [PubMed: 22323446]

53. Liu Y, et al. , The Proapoptotic F-box Protein Fbxl7 Regulates Mitochondrial Function by Mediating the Ubiquitylation and Proteasomal Degradation of Survivin. J Biol Chem, 2015. 290(19): p. 11843–52. [PubMed: 25778398]

54. Hebert AS, et al. , Improved Precursor Characterization for Data-Dependent Mass Spectrometry. Anal Chem, 2018. 90(3): p. 2333–2340. [PubMed: 29272103]

55. Jurczak MJ, et al. , Dissociation of inositol-requiring enzyme (IRE1alpha)-mediated c-Jun N-terminal kinase activation from hepatic insulin resistance in conditional X-box-binding protein-1 (XBP1) knock-out mice. J Biol Chem, 2012. 287(4): p. 2558–67. [PubMed: 22128176]
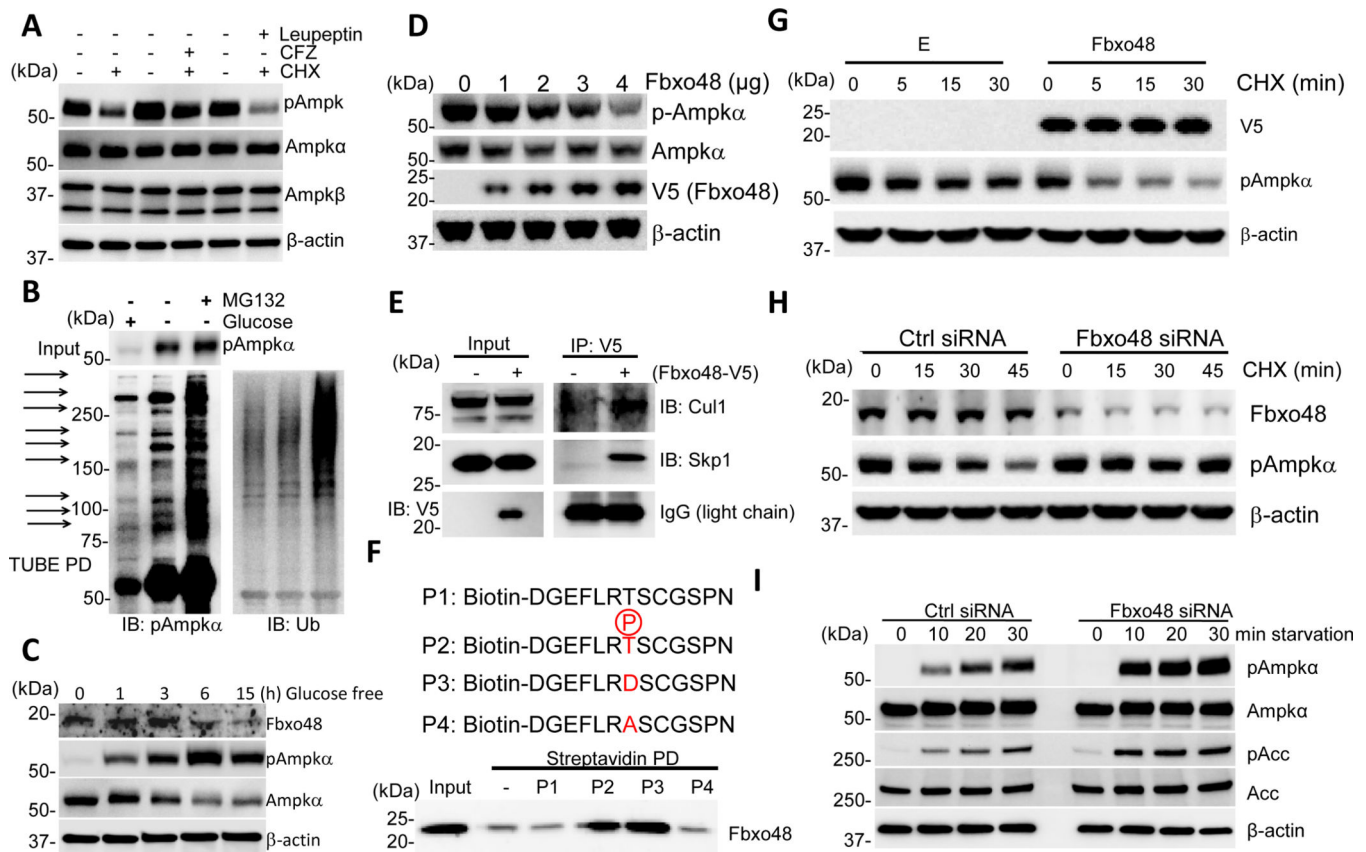
Fig. 1. pAmpkα undergoes SCF^Fbxo48 mediated ubiquitin proteasomal degradation.
(**A**) BEAS-2B cells were pretreated with glucose free DMEM 2% media, including DMSO alone (control, Ctrl), with Carfilzomib ([CFZ], 1 μM) or leupeptin (20 μM) for 30 min, then CHX (40 μg/ml) was added for additional 30 min, cells were collected for immunoblot analysis (Results are representative of three independent experiments). (**B**) BEAS-2B cells were pretreated in glucose free media with or without MG132 (20 μM) for 1 h. Whole cell extracts were subjected to TUBE agarose beads pull down (PD) and immunoblotting. Cells in glucose-rich full media served as a negative control. Arrows indicate polyubiquitylated products. Ub: ubiquitin (Results are representative of three independent experiments). (**C**) BEAS-2B cells were cultured in glucose free DMEM 2% media at indicated times. Whole cell lysates were subjected to immunoblotting (Results are representative of three independent experiments). (**D**) BEAS-2B cells were nucleofected with increasing amounts of V5 tagged *Fbxo48* plasmids. After 60 h incubation, cells were then exposed to 2% DMEM media without glucose before immunoblotting (Results are representative of three independent experiments). (**E**) BEAS-2B cells were nucleofected with empty vector or *Fbxo48*-V5 plasmid. 48 h later, cell lysates were subjected to immunoprecipitation (IP) using V5 antibodies and IP output was assayed with immunoblotting (Results are representative of two independent experiments). (**F**) Biotin labeled Ampkα peptides were first bound to streptavidin beads. Ampk beads were then incubated with purified recombinant Fbxo48 protein for 2 h. Beads were then washed, and protein was eluded before immunoblotting (Results are representative of two independent experiments). (**G**) BEAS-2B

cells were nucleofected with 2 μg of either empty vector or *Fbxo48*-V5 plasmid. 48 h later, cells were exposed to glucose free 2% DMEM media for 1 h, and then CHX (40 μg/ml) was added at indicated time points. Cells were collected for immunoblotting (Results are representative of two independent experiments). **(H)** BEAS-2B cells were nucleofected with control or *Fbxo48* siRNA. After 72 h incubation, cells were treated with CHX and assayed for immunoblot (Results are representative of two independent experiments). **(I)** BEAS-2B cells were nucleofected with 50 pg control or *Fbxo48* siRNA. After 72 h incubation, cells were treated in glucose free media for a time course before assayed for immunoblotting (Results are representative of three independent experiments).
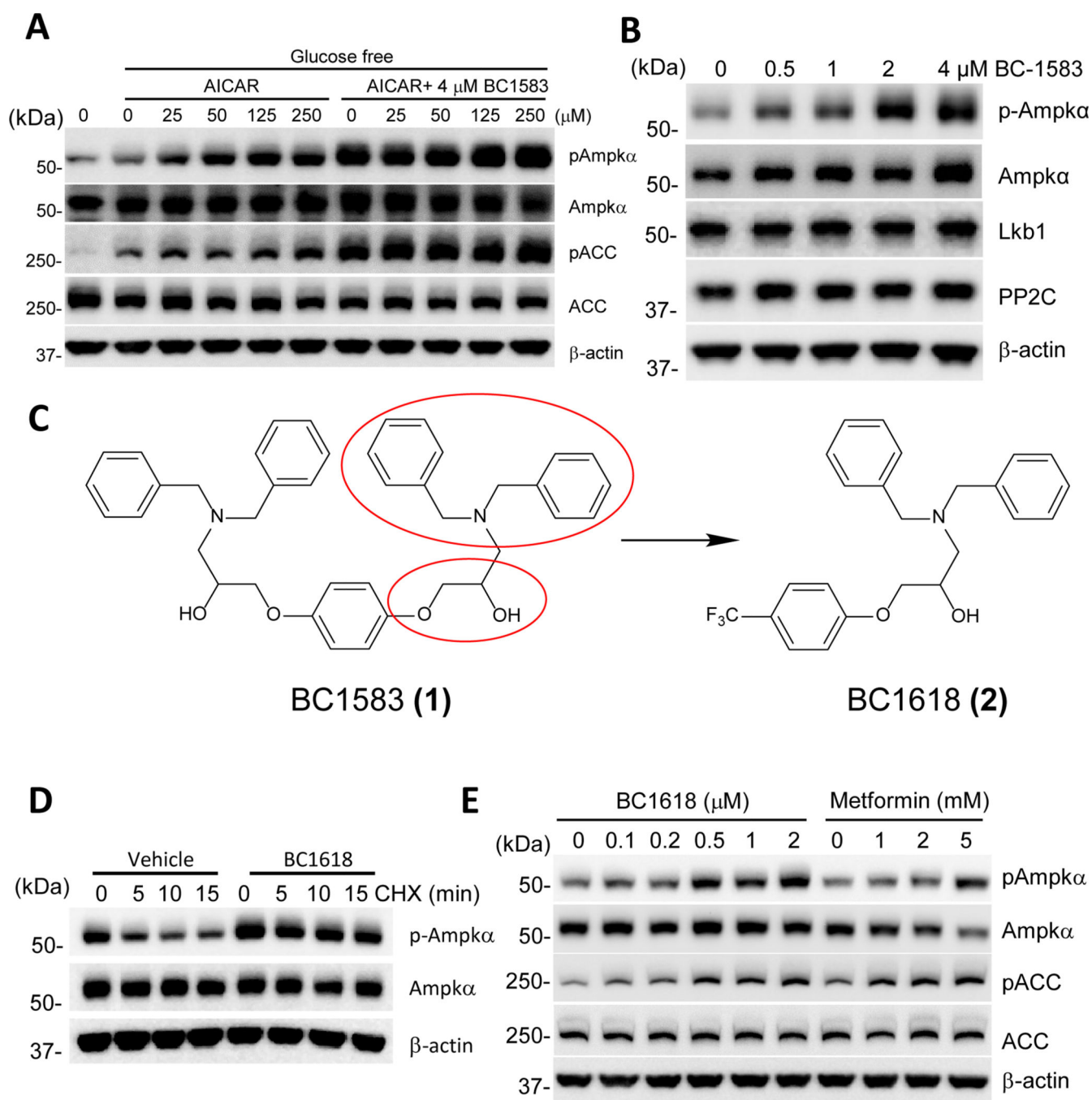
Fig. 2. Small molecule Fbxo48 inhibitors increase pAmpkα.
(**A**) BEAS-2B cells were incubated in glucose free 2% DMEM media for 16 h containing AICAR at indicated concentrations, with or without 4 μM BC1583. Non-treated cells cultured in glucose containing full media served as a negative control. Cell lysates were subjected to immunoblotting (Results are representative of three independent experiments). (**B**) BEAS-2B cells were cultured in glucose free 2% DMEM media overnight with various concentrations of BC1583 before immunoblotting (Results are representative of four independent experiments). (**C**) The hit compound BC1583 and its analog BC1618.

Red circles illustrate the essential signatures of the molecule. **(D)** BEAS-2B cells were pretreated with BC1618 (10 µM) for 2 h in full media. Media were then switched to glucose free 2% DMEM media for additional 1 h incubation. CHX (40 µg/ml) was then added at indicated time points before immunoblotting (Results are representative of three independent experiments). **(E)** BEAS-2B cells were incubated in glucose free 2% DMEM media containing either BC1618 or metformin at indicated concentrations for 16 h. Cell were collected for immunoblotting (Results are representative of five independent experiments).
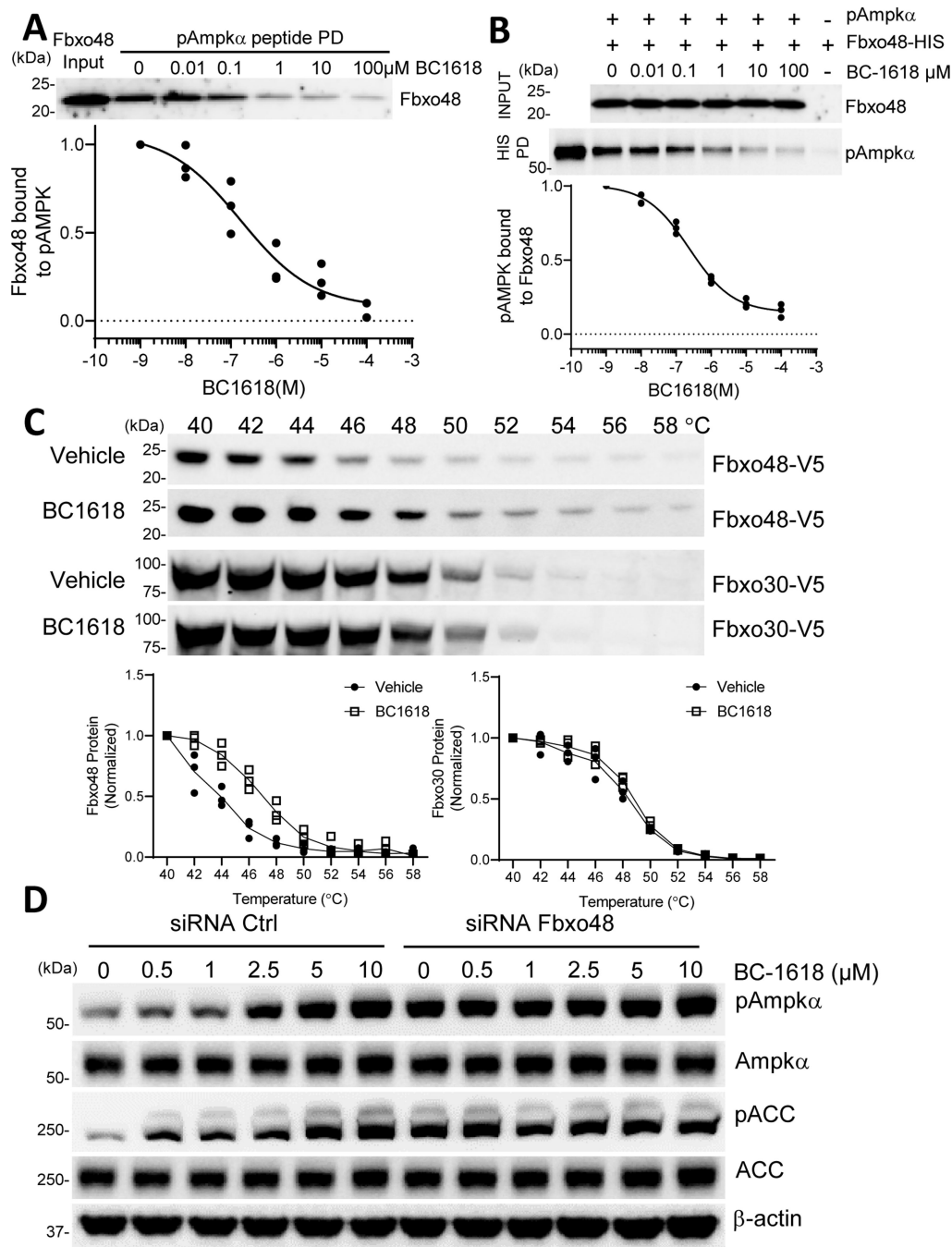
Fig. 3. Fbxo48 inhibitor interrupts Fbxo48/pAmpkα interaction.
(A) 10 μg phospho-Ampkα peptide (Biotin-DGEFLRT(p)SCGSPN) was used as bait for recombinant Fbxo48 capture and PD with streptavidin in the presence of BC1618 titration (Results are representative of three independent experiments). **(B)** 1 μg recombinant Fbxo48 (HIS-tagged) protein was used as bait for recombinant pAmpkα capture and PD with HIS beads in the presence of BC1618 titration (Results are representative of three independent experiments). **(C)** Cell based thermal shift assay (CETSA) of Fbxo48-V5 and Fbxo30-V5 proteins in HEK293 cells treated with BC1618 (3μM) or DMSO (Results are representative

of three independent experiments). The graphs below show differential ability of BC1618 to raising the thermal stability curve of Fbxo48 unlike control Fbxo30. **(D)** BEAS-2B cells were nucleofected with 50 pg control siRNA or *Fbxo48* siRNA. After 72 h incubation, cells were exposed to BC1618 in a concentration dependent manner in glucose free 2% DMEM media for 6 h before immunoblotting (Results are representative of three independent experiments).
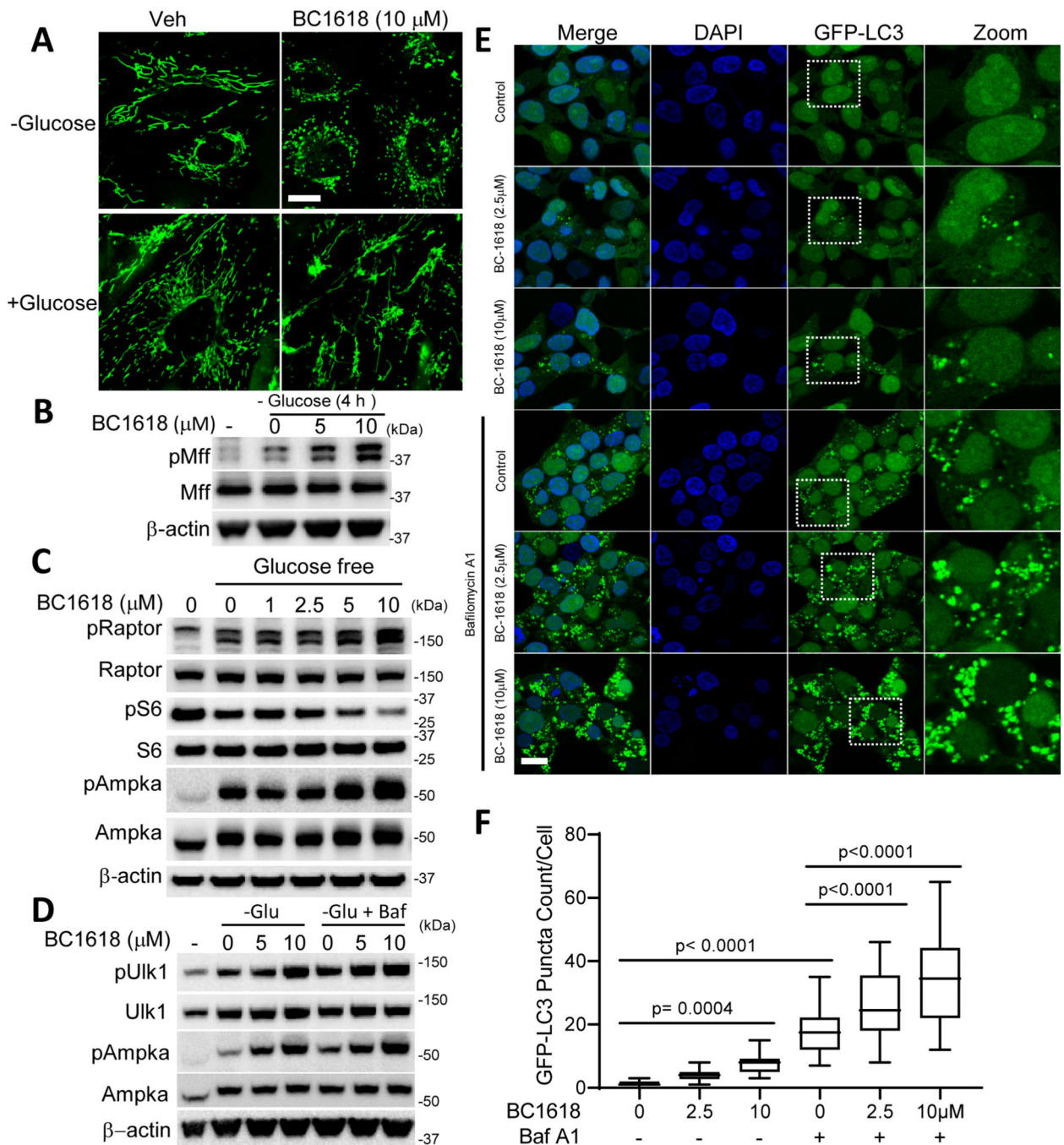
Fig. 4. BC1618 facilitates mitochondria fission and autophagy.

(**A**) BEAS-2B cells were exposed to either DMSO (vehicle, Veh) or BC1618 (10 μM) in 2% DMEM media with or without glucose for 5 h. Cells were then stained with 100 nM Mitotracker Green FM for 25 min before confocal microscopy. Scale bar=10 μm (Results are representative of two independent experiments). (**B**) BEAS-2B cells were exposed to BC1618 at indicated concentrations in glucose free 2% DMEM media for 4 h before immunoblotting. Cells in high glucose media served as controls (Results are representative of three independent experiments). (**C**) BEAS-2B cells were incubated in

glucose free 2% DMEM media containing BC1618 at indicated concentrations for 6 h before immunoblotting. Cells in high glucose media served as controls (Results are representative of three independent experiments). **(D)** BEAS-2B cells were exposed to BC1618 in glucose free 2% DMEM media with or without Bafilomycin A1 (Baf, 50 nM) for 4 h before immunoblotting. Non-treated cells in high glucose media represented the control group (Results are representative of two independent experiments). **(E)** HEK293A cells stably expressing GFP-LC3 were incubated in 2% high glucose DMEM media containing Baf (2.5 nM) with or without BC1618 for 24 h. Cells were fixed in 4% paraformaldehyde/PBS for 15 min before DAPI staining. Cells were then subjected to confocal microscopic analysis (Results are representative of three independent experiments). Scale bar = 10 μm. **(F)** Puncta from 50 randomly picked cells of each group from **(E)** were counted and plotted. Box plot quantification represent median and interquartile range with P-value range indicated by one-way ANOVA with Tukey's test of multiple comparisons (F).
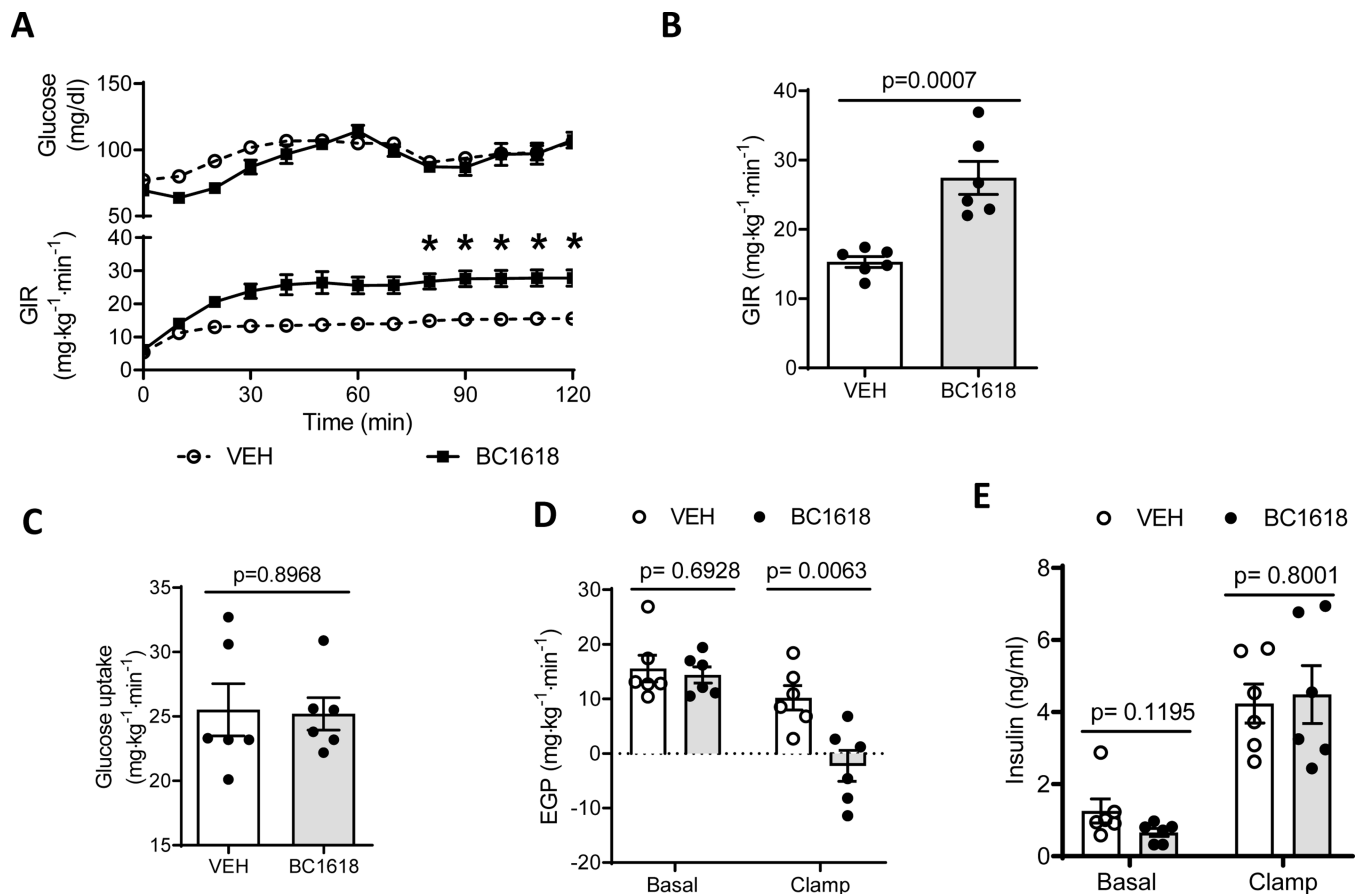
Fig. 5. BC1618 improves hepatic insulin sensitivity in diet-induced obese mice.
(A) Plasma glucose levels (upper panel) and the glucose infusion rate (GIR; lower panel) required to maintain euglycemia during a hyperinsulinemic infusion. Data are mean ± s.e.m. for n=6 per group; 80 min, p=0.0390; 90 min, p=0.0344; 100min, p=0.0384; 110min, p=0.0398; 120min, p=0.0398, as determined by two-way ANOVA with Sidak's test of multiple comparisons. **(B)** GIR during steady-state or the last 40 min of the 120 min study, data are mean ± s.e.m. for n=6 per group and were compared by unpaired, two-tailed Student's t-test.**(C)** Rates of whole-body insulin-stimulated glucose uptake during steady-state, data are mean ± s.e.m. for n=6 per group and were compared by unpaired, two-tailed Student's t-test.**(D)** Rates of basal and insulin-stimulated endogenous or hepatic glucose output (EGP) during the study, data are mean ± s.e.m. for n=6 per group and were compared by unpaired, two-tailed Student's t-test. **(E)** Basal and clamped plasma insulin levels, data are mean ± s.e.m. for n=6 per group and were compared by unpaired, two-tailed Student's t-test.